# MicroRNA166-HD-ZIP III module impacts tuber shape, color and productivity in potato

Nikita Sunil Patil[1], Arati Vasav[1], Jyoti Kumari[1], Gourav Arora[1,2], Bhavani Natarajan[1,3] and Anjan K. Banerjee[1*]

[1] Biology Division, Indian Institute of Science Education and Research (IISER) Pune, Dr. Homi Bhabha Road, Maharashtra, India

[2] Department of Plant Developmental Biology, Max Planck Institute for Plant Breeding Research, Cologne, Germany

[3] Department of Plant Sciences, University of Cambridge, Downing Street, Cambridge CB2 3EA, UK

* Corresponding author

Prof. Anjan K. Banerjee

E-mail: akb@iiserpune.ac.in

Tel: +91-20-25908057

The author responsible for distribution of materials integral to the findings presented in this article in accordance with the policy described in the Instructions for Authors (https://academic.oup.com/plphys/pages/General-Instructions) is Prof. Anjan K. Banerjee.

**Summary**

MicroRNA165/166 is a highly conserved and abundant microRNA family in plants that targets class III homeodomain leucine zipper (*HD-ZIP III*) transcription factors. Their essential roles in plant development, organ polarity, meristem maintenance, and vascular differentiation have been well established. However, their role in storage organ development, particularly in potato tuberization remains unknown. Here, we demonstrate the pleiotropic effects of *miR166* on potato (*Solanum tuberosum* spp. *Andigena*) growth and development. Suppression of *miR166* via target mimicry (MIM166) resulted in reduced plant height, altered vascular patterning, diminished leaf curvature, and impaired root development. Remarkably, MIM166 lines produced elongated, pigmented tubers with reduced yield under short-day conditions. Transcriptomic analyses of swollen head *versus* stalk of tuberizing stolons revealed altered expression of auxin-, cytokinin-, and gibberellin-related genes, consistent with hormone quantification data, suggesting the key role of phytohormones in governing tuber shape. Anthocyanin profiling indicated elevated accumulation of cyanidin 3-glucoside, pelargonidin 3-glucoside, and delphinidin 3-glucoside in MIM166 tuber peels, correlating with the upregulation of anthocyanin biosynthetic genes. Tuber productivity in these lines was reduced possibly due to the decreased expression of *SWEET11b* and distorted vascular structures in the MIM166 lines. Further, *StREVOLUTA*, a direct miR166 target, exhibited dynamic expression during stolon differentiation and could modulate the expression of auxin biosynthesis genes. Collectively, our results demonstrate that the *miR166-HD-ZIP III* module is functional in potato, plays conserved roles in regulating key developmental traits, and is active through early stolon-to-tuber transition stages, affecting tuber shape, color and productivity.

**Significance statement**

The microRNA166–HD-ZIP III regulatory module plays a central role in plant growth and development. However, its function in tuber/ storage organ development remains unexplored. Here, we show that the miR166–HD-ZIP III has distinct regulatory roles in potato, influencing tuber shape, pigmentation, and yield. These findings reveal previously unrecognized functions of the miR166–HD-ZIP III module in tuber crops and broaden our understanding of miR166-mediated developmental regulation in plants.

**Key words:** miR166, HD-ZIP III, Potato, Tuber shape, Anthocyanin, auxin, REVOLUTA

## Introduction

MicroRNA 165/166 (miR165/166), a highly conserved family of microRNAs (miRNAs), play important roles in regulating a wide range of physiological processes in plants. They target specific transcription factors (TFs)- members of the *Homeodomain-Leucine Zipper Class III* (*HD-ZIP III*) gene family, that are shown to critically regulate processes such as embryo patterning, development of leaf, roots, vasculature and apical meristems, and establishment of organ polarity, making the *miR166-HD-ZIP III* module central to plant growth and morphogenesis (Turchi *et al*., 2015; Ramachandran *et al*., 2017; Roodbarkelari., 2017). *miR166* is also involved in mediating plant responses to various abiotic stresses such as drought, salinity, and temperature fluctuations (Yadav *et al*., 2021; Wang *et al*., 2025; Wei *et al*., 2025). Several studies have demonstrated the potential of *miR166* as an important candidate in agricultural biotechnology, wherein its manipulation could improve crop resilience and productivity (Boualem *et al*., 2008; Zhang *et al*., 2018; Zhao *et al*., 2022).

*miR165/166* and their target genes are extensively studied in *Arabidopsis*, and to some extent in crop plants such as rice, maize, tomato, peach, soybean, tea, and legumes (Boualem *et al*., 2008; Valiollahi *et al*., 2014; Zhang *et al.,* 2015; Ding *et al*., 2018; Zhang *et al*., 2018; Li *et al*., 2020; Zhao *et al*., 2022; Zhou *et al*., 2024). In *Arabidopsis*, *miR165* (miR165a and miR165b) and *miR166* (miR166a-miR166g) target five genes that encode HD-ZIP III TFs- *PHABULOSA* (*PHB*), *PHAVOLUTA* (*PHV*), *REVOLUTA* (*REV*), *ATHB-8*, and *ATHB-15*/*CORONA* (*CRN*)/*INCURVATA4* (*ICU4*). These TFs are closely related, and are known to play both overlapping and antagonistic roles in various biological processes (Prigge *et al*., 2005). Overexpression of *miR165* causes a drastic reduction in all five *HD-ZIP III* genes in *Arabidopsis*, recapitulating the phenotypes caused by loss-of-function mutations of HD-ZIP III, such as distorted shoot apical meristem (SAM), altered organ polarity, and defects in the development of vascular tissues and interfascicular fibers (Zhou *et al*., 2007). In tomato, HOMEOBOX15A (SlHB15A) acts as a key regulator for preventing fruit set in the absence of fertilization. *SlHB15A* loss-of-function produces parthenocarpic fruits under both optimal and heat stress conditions due to aberrant ovule development (Clepet *et al*., 2021). In soybean, knockdown of *miR166*

102 (*GmSTTM166*) causes increased expression of *ATHB14-LIKE*, reduces plant height,
103 and lowers the levels of bioactive gibberellic acid ($GA_3$). ATHB14-LIKE directly
104 represses transcription of *GmGA1* and *GmGA2* (GA biosynthesis genes), while
105 activates the transcription of the GA catabolic gene *GmGA2ox2* (Zhao *et al*., 2022).
106 Thus, *miR166* plays a pivotal role in crop plants as it regulates key agronomic traits
107 such as plant height, fruit set, and stress responses that ultimately affect yield.

108 Potato tuberization is a complex process governed by several molecular
109 signals such as small RNAs, transcription factors, proteins, phytohormones, and
110 sucrose. The mobile signals such as *StBEL5*, StSP6A, StPTB1, StPTB6 and others are
111 systematically transported from leaves to belowground stolons under inductive
112 conditions to initiate tuber development (Hannapel *et al*., 2017). Overexpression of
113 *miR156* causes development of aerial tubers from axillary meristems while
114 overexpression of *miR172* abolishes SD-dependency of tuberization (Martin *et al*.,
115 2009; Bhogale *et al*., 2014). Further, a phasiRNA *siRD29(-)* is shown to fine-tune
116 *StGA3ox3* levels during stolon-to-tuber transitions (Malankar *et al*., 2023). In potato,
117 the miR166 family is amongst the most abundantly expressed miRNAs, with a total
118 transcript per million exceeding 600,000, and exhibits tissue-specific and stolon-to-
119 tuber stage-specific expression profiles (Lakhotia *et al*., 2014; Kondhare *et al*., 2018).
120 During further analysis of the small RNA sequencing data from Kondhare *et al.*
121 (2018), we found *miR166* to be differentially accumulated under long-day (LD; 16 h
122 light/8 h dark; tuber non-inductive) and short-day (SD; 8 h light/16 h dark; tuber
123 inductive) photoperiod. This observation prompted us to investigate the role of
124 *miR166* in potato development, and tuberization in particular. Despite the diverse
125 roles attributed to *miR166* in several plants' development, productivity, and stress
126 responses, its functional characterization in potato and relevance in storage organ
127 development remains unexplored. Here, we validated the functional role of the
128 *miR166–HD-ZIP III* module in potato. Our findings show that suppression of *miR166*
129 leads to pleiotropic effects on overall plant development, highlighting its conserved
130 regulatory function across plants. Importantly, we reveal that *miR166* modulates key
131 agronomic traits in potato- tuber shape, color, and productivity.

132

133 **Results**

134

135 **Identification, validation and expression analysis of miR166 in Potato**

136 All four precursors of microRNA166 from the miRBase (the microRNA database;
137 http://mirbase.org/) are predicted to form a secondary hairpin loop structure with
138 mature 166 in its stem region (MFold; Zuker, 2003) (Figure S1A). To validate the
139 presence of miR166 precursors (precursors a, b, c and d) in potato, RT-PCR was
140 performed and the amplified products were sequence confirmed (Figure 1A).
141 Precursor-b was the least abundant form, as compared to the other three precursors.
142 Compared to LD, the levels of precursors-a and -c decreased in the stolons under SD
143 photoperiod, while precursor-d increased (Figure 1B-D). The mature forms of all the
144 precursors are identical, except for pre-miR166b, wherein it differs by a single base
145 (Figure S1B). In our analysis of small RNA sequencing data from a previous study,
146 we found miR166 to be the most abundant microRNA in early stolon-to-tuber
147 transition stages and exhibited differential accumulation under short-day (SD; tuber
148 inductive) photoperiod (Kondhare *et al*., 2018) (Figure S2A-B). We detected the 21-
149 bp mature miR166 by stem-loop endpoint PCR from leaves and stolons of WT potato
150 plants (Figure 1E). The amplified product was verified by sequencing, thus
151 confirming that mature miR166 is expressed in potato.
152 To determine whether photoperiod affects the expression/accumulation of
153 miR166, plants were grown in soil under early long-day (LD; tuber non-inductive)
154 and SD conditions. Stem-loop quantitative reverse transcription (qRT) -PCR analysis
155 revealed a reduced accumulation of miR166 in leaves under SD conditions, while
156 stolons had comparable levels of miR166 under both the photoperiods (Figure 1F).
157 Stolons differentiating into tubers exhibited 10-40 percent reduction in the later stages
158 of stolon-to-tuber transition (Figure 1G). *In silico* analysis suggested that miR166 in
159 potato potentially targets six *HD-ZIP III* members, similar to *Arabidopsis*. Using
160 modified 5′ RLM-RACE, we mapped the cleavage site on the HD-ZIP transcripts
161 (Figure 1H), confirming the targets of miR166. Overall, our results validate the
162 existence of miR166-*HD-ZIP III* module in potato and the miR166 showed tissue-
163 specific accumulation under photoperiodic conditions.
164
165 **Knockdown of microRNA166 causes pleiotropic phenotypic changes**
166 Using a target mimicry approach, we generated stable transgenic lines of miR166 in *S.*
167 *tuberosum andigena ssp.* (Figure S3A). Of them, 2 independent lines (referred as KD
168 #2 and KD #3) exhibiting 50-75% suppression of mature miR166 were selected for
169 further characterization (Figure 2A-B). miR166 KD lines (MIM166) had reduced

170 shoot height but number of nodes remained unchanged, implying a decreased inter-
171 nodal distance, compared to the WT plants (Figure 2C-E). The leaf lamina from
172 miR166 KD lines appeared flat, hence we calculated the longitudinal and transverse
173 curvature indices ($CI^L$ and $CI^T$) (Liu *et al*., 2010) to quantify the curvature. A
174 curvature index of zero suggests that the leaf surface is completely flat. Both
175 curvature indices, $CI^L$ and $CI^T$ of the KD lines were significantly reduced compared to
176 WT (Figure 2F-G). The total chlorophyll content in the miR166 KD lines were
177 comparable to that of WT leaves; and leaves of KD #2 showed a slight increased
178 anthocyanin accumulation, relative to the WT (Figure S3B). The vascular structures
179 were distorted and had fewer xylem elements compared to the WT plants (Figure 2H).
180 Further, an i*n vitro* root growth assay revealed that the MIM166 lines had decreased
181 root length, shoot and root biomass, number of adventitious and lateral roots (Figure
182 S3C-H). Thus, several phenotypic characters were altered upon constitutive and
183 ubiquitous suppression of miR166 in potato.
184
185 **Suppression of miR166 alters tuber shape, color and productivity**
186 To examine the effect of miR166 suppression on tuber development, we subjected the
187 miR166 KD lines to tuber inductive SD photoperiod in soil conditions. Compared to
188 WT plants, the KD lines showed reduced tuber productivity in varying degrees,
189 although the number of tubers per plant did not vary significantly (Figure 3A-C).
190 Interestingly, tubers from these KD lines were elongated as opposed to the WT
191 spherical tubers. The sphericity index for these tubers was greater than 1.5, while WT
192 tubers had the sphericity index of around 1.0 (Figure 3D). However, the tuber volume
193 of KD #2 was slighty reduced when compared to WT (Figure 3E). Starch estimation
194 assay showed no significant differences in the starch accumulation in tubers of any
195 KD lines, compared to the WT tubers (Figure 3F).
196 *BEL5* and *Identity of Tuber 1* (also known as *BRC1b*) are key positive
197 regulators of tuberization (Chen *et al*., 2003; Tang *et al*., 2022). Relative
198 quantification analyses from stolons of miR166 KD lines showed a slight reduction in
199 *BEL5* and no significant changes in *IT1* levels (Figure 3G). In potato, SP6A and
200 SWEET11b are crucial for instrumenting symplastic sucrose loading under tuber-
201 inductive conditions (Abelenda *et al*., 2019). *SWEET11b* was found to be significantly
202 reduced in the stolons of both KD lines, along with varying levels of *SP6A* (Figure
203 3G). HY5 binds to the promoters to regulate the expression of *SWEET11* and

204 *SWEET12* in *Arabidopsis* (Chen *et al*., 2016; Sakuraba and Yanagisawa, 2018).
205 Stolons from KD plants had reduced *HY5* levels compared to the WT (Figure 3G).
206 Further, we found that the tuberization potential of these KD lines was greatly
207 reduced (80-100% reduction) under *in vitro* tuber inductive conditions (Figure 3H).
208 Overall, the KD lines exhibited reduced tuberization potential *in vivo* and *in vitro*,
209 accompanied with down regulation of key marker genes.
210

211 **RNA-Seq analysis revealed differentially expressed genes in swollen and sub-**
212 **swollen part of tuberizing stolons**

213 The phenotype of elongated and pigmented tuber was evident from the early stages of
214 tuber development (Figure 4A). To identify the genes associated with the phenotype,
215 we carried out paired-end RNA sequencing on two distinct regions—the swollen
216 region (Head) and the sub-swelling region (SSR)—from both WT and KD #3 samples
217 (Figure 4B; Figure S4A). The WT_Head and SSR had 37 and 376 uniquely expressed
218 genes respectively, and KD_Head and SSR had 115 and 120 uniquely expressed
219 genes respectively (Figure 4C). A comparison between the Head vs SSR tissue
220 revealed 8680 DEGs (4504 up- and 4176-down regulated) in the WT; while 7846
221 DEGs (3830 up- and 4016-down regulated) in the KD samples (Figure S4B-C; Table
222 S1-S2).

223 Using a cut-off of log2 fold change greater than 1 and p-value less than 0.05,
224 KD_Head and SSR had 9774 and 10,209 DEGs compared to respective WT_Head
225 and SSR tissues (Figure S4D-E; Table S3-S4). Variance stabilized transformed (VST)
226 values were used to visualize the gene expression patterns of certain key regulators of
227 tuberization (Figure 4D). Notably, positive regulators such as *BEL5* and *CDF1* were
228 slightly down regulated in KD, relative to WT. *SWEET11b* levels were greatly
229 reduced in both the KD tissues; while *SP6A* and *IT1* were specifically down regulated
230 in the SSR region. RT-qPCR analysis of few marker genes such as *BEL5*, *SP6A* and
231 *HY5* corroborated with the RNA-seq data (Figure S4F-H).
232

233 **Quantitative trait loci genes for tuber shape are differentially expressed in the**
234 **swollen stolons of miR166 KD plants**

235 The developmental differences between round and elongated tuber shapes begin as
236 early as the hook stage of the stolon. One of the major Quantitative trait locus (QTL)
237 for tuber shape and eye depth is located on chromosome 10 (Lindqvist-Kreuze *et al*.,

238 2015; Fan *et al*., 2022). Gene families linked to cell structure and function—such as
239 homeobox, expansins, extensins, and those involved in pectin biosynthesis and
240 modification—are particularly relevant to tuber shape and eye depth. In our
241 sequencing data, we could detect significant up regulation of plant invertase/pectin
242 methylesterase inhibitor (PMEI) superfamily protein (Soltu.DM.10G019700). The
243 PMEI members are key for balancing cell wall plasticity and rigidity. Further, HEAT
244 repeat/WD domain, G-beta repeat protein (Soltu.DM.10G019120), GRAS family
245 transcription factor (Soltu.DM.10G020490), NB-ARC domain-containing disease
246 resistance protein (Soltu.DM.10G016590) and heat shock protein 70B
247 (Soltu.DM.12G011130) were significantly down regulated in the KD_Head, but not
248 in the SSR (Figure 4E; Figure S5A; Table S3-S4).

249 The Round (Ro) locus is a major genetic determinant of tuber shape (round vs.
250 long/cylindrical) that maps to chromosome 10 in potato and behaves as a major-effect
251 QTL for length:width ratio. A total of 18 genes from the Round (Ro) region were
252 identified in a previous study (Fan *et al*., 2022), of which we could detect 16 genes in
253 our RNAseq data. Of these, notably Leucine-rich repeat protein kinase family protein
254 (Soltu.DM.10G018490, Soltu.DM.10G018500), Glycosyl hydrolase superfamily
255 protein (Soltu.DM.10G018520), Aminophospholipid ATPase (Soltu.DM.10G018550),
256 Polynucleotidyl transferase, ribonuclease H-like superfamily protein
257 (Soltu.DM.10G018600), and HSI2-like (Soltu.DM.10G018620,
258 Soltu.DM.10G018640) were found to be significantly down regulated in the
259 KD_Head relative to WT_Head (Figure 4F; Table S3). Most of these genes followed
260 a similar expression trend in the KD_SSR tissue. (Figure S5B; Table S4). Only one
261 member belonging to the Ovate family protein (OFP)- StOFP20
262 (Soltu.DM.09G010420) has been characterized in potato (Ju *et al*., 2023), wherein
263 altering its expression changes tuber shape likely through interactions that control cell
264 division/expansion. In the KD_Head, we found multiple OFP members such as
265 Soltu.DM.01G003200, Soltu.DM.01G031520, Soltu.DM.03G004280,
266 Soltu.DM.05G025790, Soltu.DM.06G032770, Soltu.DM.09G010420,
267 Soltu.DM.10G025300, Soltu.DM.10G025310, Soltu.DM.11G022190,
268 Soltu.DM.12G024960 to be significantly up regulated; while in the KD_SSR, certain
269 other OFP members- Soltu.DM.02G025370, Soltu.DM.09G024410 and
270 Soltu.DM.11G006960 showed strong differential expression relative to WT (Figure
271 S5C; Table S3-S4).

272

273 **Tuberizing stolons exhibit differential expression of phytohormone-associated**
274 **genes and accumulation of hormone in swollen vs. SSR region**

275 A comparison between the Head and SSR tissues from WT and KD revealed
276 significant changes in the expression patterns of hormone-related genes (Figure 5A-B;
277 Figure S6A-B). In WT, auxin biosynthesis genes - *StTAA-like*, *StYUCCA4* and
278 *StYUCCA8* were up regulated in the Head compared to the SSR. This spatial
279 expression distinction was lost in the KD line. Also, *StYUCCA5a* and *StYUCCA7*
280 exhibited reversed expression patterns in KD line relative to WT. Auxin transport
281 genes- *StPIN2/4/8/9* displayed markedly altered expression patterns in KD tissues,
282 suggesting perturbed auxin distribution (Figure 5A; Figure S6A). The gibberellin (GA)
283 biosynthesis genes *StGA3ox3* and *StGA20ox2* were found to be up regulated in both
284 the KD tissues (Figure 5A; Figure S6A). Also, the differential expression of the GA
285 catabolic gene *StGA2ox1*, which was evident between Head and SSR in WT, was
286 abolished in the KD line. Expression of the cytokinin (CK) biosynthesis genes
287 *StIPT3/5* and *StCYP735A* was altered and that of *StLOG1a/3b/7c/8b* and *CKX6* in the
288 Head *vs.* SSR tissue was reversed in the KD lines (Figure 5B; Figure S6B). Cytokinin
289 transporter *PUP1-7/9* showed significant reversed expression in the Head *vs.* SSR
290 tissues of respective lines. RT-qPCR analysis of selected phytohormone-related genes
291 validated the RNA-seq results, confirming the altered expression patterns (Figure 5C;
292 Figure S6C). In line with the transcriptomic data, auxin quantification using LC-
293 MS/MS revealed similar auxin levels in both the Head and SSR regions of KD,
294 whereas WT exhibited significantly lower auxin levels in the SSR (Figure 5D; Data
295 S1.). Additionally, $GA_3$ levels in KD stolons were relatively 5.5 folds lower than
296 those in WT, indicating an altered hormone dynamics in the KD line (Figure 5E).

297

298 **Anthocyanin-related genes are differentially expressed in the tuberizing stolons,**
299 **and tuber peels show varying pigment accumulation**

300 miR166 suppression led to the development of pigmented tubers in KD #2 and KD #3
301 lines. The pigmentation was observed only in the peel of these tubers, while the flesh
302 color was comparable to WT tubers (Figure 6A). Metabolic profiling of the tuber
303 peels revealed that KD #2 had increased accumulation of cyanidin 3-glucoside, while
304 KD #3 had increased accumulation of both cyanidin 3-glucoside and pelargonidin 3-
305 glucoside, relative to WT (Figure 6B). In contrast, delphinidin 3-glucoside was

306 reduced in both the KD lines (Figure 6B). These shifts in anthocyanin profiles
307 contributed to the altered pigmentation observed in KD tubers, a trait visible from
308 early stages of tuber development (Figure 4A). Transcriptomic analysis of the Head
309 and SSR tissues from early stages of tuberization revealed that several structural and
310 accessory genes of the anthocyanin biosynthesis pathway were up regulated in the
311 KD_Head as compared to the WT (Figure 6C). A weighted correlation network
312 analysis (WGCNA) by Zhang *et al*., (2024) identified a set of TF families having the
313 highest correlation with these anthocyanin pathway genes. Few TFs- bHLH, WRKY,
314 GRAS, bZIP, LBD, ARF, B3, G2-like, HB-other, HD-ZIP, MYB, and MYB-related
315 exhibited significant differential expression in the Head tissue (Figure 6D; Table S3-
316 S4). The anthocyanin pathway genes and associated TFs were differentially expressed
317 in the SSR tissues as well (Figure S7A-B).
318
319 **miR166 overexpression exhibits minimal effects on vasculature and tuberization**
320 MicroRNA166 levels are abundant in the early stolon-to-tuber transitions and
321 decrease at the mini-tuber stage (Figure 1G). To investigate the effects of miR166
322 overexpression in potato, we generated stable transgenic lines overexpressing
323 precursor miR166-d and evaluated their overall phenotype and tuberization potential
324 under SD conditions. The overexpression (OE) lines OE #9 and #13 lines showed
325 variable levels of mature miR166 in leaf (Figure S8A-B). OE #13 exhibited a slight
326 reduction in plant height and internodal distance, while the leaf curvature and overall
327 architecture was comparable to those of WT plants (Figure S8C-F). The number of
328 vascular cells in the OE #9 shoot seemed to be increased, relative to the WT plants
329 (Figure S8G). Under SD conditions, the OE #9 exhibited a slight increase in tuber
330 productivity, although the number of tubers remained largely unchanged (Figure S8H-
331 J). RT-qPCR analysis revealed no significant difference in the levels of mature
332 miR166 in the stolons of OE lines, which may be due to the inherently high miR166
333 in the WT stolon (Figure S8K). The tuber marker gene *BEL5* did not show significant
334 variation between OE and WT stolons, while the tuber identity gene *IT1* was up
335 regulated (Figure S8L). Additionally, auxin biosynthesis and transport-related genes
336 were generally up regulated in the stolons of OE lines compared to WT (Figure S8M).
337 Thus, miR166 OE lines exhibited some phenotypic alterations, comparatively less
338 severe than miR166 KD lines.
339

340 **REVOLUTA, a miR166 target affects tuberization and influences auxin-related**
341 **genes in potato**
342 Using modified 5'RLM-RACE, we detected the miR166 cleaved fragments of *REV* as
343 predicted by psRNAtarget finder (https://www.zhaolab.org/psRNATarget/home) and
344 mapped the miR166 cleavage site (Figure 7A; Figure 1H). In the WT stolons, REV
345 transcripts were higher under long-day (LD) conditions and in shoot-forming stolons,
346 whereas SD stolons exhibited dynamic expression across different tissues including
347 the stolon, swollen region, SSR, and mini-tuber (Figure 7B). Stolons from miR166
348 KD lines had increased *REV* levels, while a slight reduction was observed in the OE
349 stolons (Figure 7C). GUS assay of the stable transgenic lines expressing
350 promREV::*uidA* showed promoter activity in the apical and axillary meristems,
351 subtending regions likely corresponding to the vascular tissue, in the swollen regions
352 of tuberizing stolons and at the apex of the mini-tuber stage (Figure 7D). Stable
353 transgenic lines of REV anti-sense (AS) exhibited variable degrees of *REV*
354 suppression in leaves and stolons (Figure S9A-B), however their overall growth and
355 architecture was comparable to WT plants (Figure 9C). The stem vasculature in REV
356 AS #6 was smaller than that of in the WT (Figure S9D). Under SD photoperiod, all
357 three AS lines displayed significantly reduced tuber yield, although the average
358 number of tubers per plant remained largely unchanged (Figure 7E-G). Thus,
359 *REVOLUTA* is a spatio-temporally regulated target of miR166 in potato, and its
360 suppression led to reduced tuber productivity. *REVOLUTA* is known to regulate the
361 expression of auxin-related genes in *Arabidopsis* (Brandt *et al*., 2012). It is shown to
362 bind the promoters of TAA1 and YUCCA5 through the AT[G/C]AT palindromic
363 sequence, which was identified as the *in vitro* binding sequence for HD-ZIP III
364 proteins (Sessa *et al*., 1998). Our *in-silico* promoter analysis of auxin biosynthesis
365 genes in potato revealed the presence of these core binding motifs within their
366 upstream regulatory regions (Figure 7H). Transient overexpression of *StREV* in potato
367 leaves reduced the transcript abundance of *StYUCCA4, -7* and *-8* genes (Figure 7I),
368 suggesting that REV might exert an inhibitory effect on the promoter activity of auxin
369 biosynthesis genes and regulate their expression.
370
371 **Discussion**
372 MicroRNAs are key regulators of plant development and defense responses, and
373 amongst them, miR166 represents a well-conserved family that targets members of

374 the HD-ZIP III transcription factors. Knockdown of miR166 in maize, rice,
375 *Arabidopsis* and tomato has been shown to affect multiple developmental traits such
376 as leaf rolling, vascular patterning, epidermis structure, tassel architecture, tiller angle,
377 yield-related traits, and abiotic stress responses (Jia *et al*., 2015; Zhang *et al*., 2018; Li
378 *et al*., 2020; Zhao *et al*., 2022). In potato, overexpression of miR156 led to the
379 development of aerial tubers under inductive SD photoperiod (Bhogale *et al*., 2014).
380 In another study, the authors showed that the polycomb group member- StMSI-1
381 alters the expression of several genes encoding histone modifiers and positively
382 regulates miR156 expression in potato (Kumar *et al*., 2020). Martin *et al*. (2009)
383 showed that overexpression of miR172 abolished the photoperiod dependency of
384 tuberization. A recent study (Malankar *et al*., 2023) demonstrated the role of a phasi
385 RNA siRD29(-) in fine-tuning the expression of *StGA3ox3* in the early stages of
386 stolon-to-tuber transition. These studies reveal the critical roles of microRNAs in
387 governing potato tuberization.
388 In our preliminary analysis of small RNA sequencing datasets (Lakhotia *et al*.,
389 2014; Kondhare *et al*., 2018), we identified miR166 as the most abundant microRNA
390 in potato stolons, suggesting its involvement in stolon-to-tuber transition stages.
391 However, to our knowledge, the functional characterization of miR166–*HD-ZIP III*
392 module in potato, specifically in the storage organ development, remains unknown.
393 Here, we demonstrate that the miR166–*HD-ZIP III* module is functional in potato,
394 plays conserved roles in regulating key developmental traits, and is active through
395 early stolon-to-tuber transition stages affecting tuber shape, color and productivity.
396
397 **The functional roles of miR166 are conserved in potato**
398 A constitutive and ubiquitous knockdown of miR166 in potato (MIM166) led to the
399 development of several pleiotropic phenotypes. The MIM166 lines had reduced plant
400 height, having no significant changes in the number of nodes (Figure 2C-E). In
401 soybean, Zhao *et al*. (2022) showed that suppression of miR166 led to decreased plant
402 height. ATHB14-LIKE (a HD-ZIP III target of miR166) promoted the expression of
403 a GA catabolic gene- *GIBBERLLIN 2 OXIDASE2*, causing decreased bioactive GA
404 levels in the plant affecting the height. In potato, MIM166 *in vitro* shoots and roots
405 had increased levels of inactive GA8 (degraded product) and elevated expression of
406 GA2ox1 in stolons, compared to the WT tissues (Figure S11A-B; Figure 5A),
407 suggesting a similar GA dynamics in potato influencing the shoot height. In

408 *Arabidopsis,* miR165/166 suppression led to pleiotropic effects on leaf development
409 such as trumpet-shaped leaves, ectopic leaflets on the abaxial side, increased leaf
410 numbers and accumulation of purple pigment (Jia *et al*., 2015). Knockdown lines of
411 miR166 in rice exhibited a rolled-leaf phenotype, having smaller bulliform cells and
412 abnormal sclerenchymatous cells (Zhang *et al*., 2018). In potato, MIM166 lines
413 exhibited reduced curvature of the leaf blades, variations in the total leaflet length and
414 number of lateral leaves (Figure 2F-G; Figure S11C). Thus, miR166 suppression
415 causes diverse leaf phenotypes in different plants, suggesting a conserved yet species-
416 specific role in regulating leaf development.
417 Two targets of miR166, ATHB15 and HB8, play antagonistic roles in the
418 regulation of xylem development in *Arabidopsis* (Baima *et al*., 2001; Kim *et al*.,
419 2005). *ATHB15* is exclusively expressed in vascular tissues and its suppression leads
420 to expanded xylem tissue and inter-fascicular region, indicative of accelerated
421 vascular cell differentiation from cambial/procambial cells (Kim *et al*., 2005). We
422 observed that stable potato transgenic lines of miR166 (MIM and OE) had altered
423 vascular structures in the stem (Fig 2H; Figure S8G), suggesting miR166-*HD-ZIP III*
424 network might also influence differentiation of vascular cells in potato. Singh *et al*.
425 (2014) showed that phytohormones dynamically regulate the expression of
426 miR165/166 in roots of *Arabidopsis*, and control root meristem size and growth. *In*
427 *vitro* root growth assay of potato MIM166 lines showed decreased root length, root
428 biomass, number of adventitious and lateral roots (Figure S3C-H), suggesting the
429 essential role of miR166 in root development of potato. Overall, these pleiotropic
430 phenotypes of the potato MIM166 lines recapitulate the phenotypic traits observed in
431 other plants, and highlight its conserved functional roles as a central regulator of
432 growth and development.
433
434 **miR166 impacts tuber shape, color, and productivity in potato**
435 Phytohormone quantification, RNA sequencing of tuberizing stolons (Head *vs.* SSR),
436 and anatomical and molecular analyses revealed crucial insights into the altered tuber
437 phenotypes of MIM166 plants. Phytohormones such as auxin and GA influence fruit
438 shape in tomato and apple. Stembridge and Morrell (1972) showed that spraying $GA_4$,
439 $GA_7$, and 6-BAP increased the length/diameter ratio in apples, while Wang *et al*.
440 (2019) showed that auxin application before anthesis produced elongated tomato
441 fruits. $GA_3$ application promotes organ elongation and delays ripening, whereas

442 paclobutrazol reduces fruit shape index and shortens ripening time in tomato (Chen *et*
443 *al*., 2020). In potato stolons, high GA levels inhibit tuberization, while auxin content
444 increases under inductive conditions. *StGA3ox3*, a GA biosynthesis gene, is active in
445 the tuber heel and regulates stalk formation (Malankar *et al*., 2023). In our study, the
446 GA catabolic gene *GA2ox1* was up regulated (Figure 5A), accompanied by a 5.5-fold
447 reduction in bioactive $GA_3$ in MIM166 stolons (Figure 5E). Genes involved in auxin
448 biosynthesis (*StTAA-like, StYUCCA4/5a/7/8*) and transport (*StPIN2/4/8/9*) showed
449 altered expression in KD_Head vs. WT_Head, suggesting disrupted auxin distribution.
450 Consistently, auxin levels in KD Head vs. SSR were comparable, unlike the distinct
451 accumulation in WT (Figure 5D). Cytokinin, which is essential for cell division and
452 expansion during tuber bulking (Mingo-Castel *et al*., 1976; Sattelmacher and
453 Marschner, 1978), had reduced expression of its biosynthesis and transport genes in
454 SSR, possibly affecting the radial cell expansion. Moreover, MIM166 tuber sprouts
455 were stunted, pigmented, and highly branched (Figure S6D), indicating an altered
456 auxin–CK dynamics (Muller and Leyser, 2011). We propose that disrupted auxin–
457 GA–CK balance in differentiating stolons caused elongated tubers in MIM166 plants.
458 Further analysis of our transcriptomic data sets revealed that genes located
459 within QTLs on chromosomes 5, 10, and 12—associated with tuber shape and eye
460 depth— are differentially expressed. Several PMEI members, GRAS transcription
461 factors, and disease resistance genes were downregulated in KD_Head relative to WT
462 (Figure 4E; Figure S5A; Tables S3–S4). PMEIs can modulate invertase activity and
463 sugar metabolism (Lin *et al*., 2015; Draffehn *et al*., 2010), while pectin
464 methylesterase activity affects pectin structure and tuber texture (Ross *et al*., 2010),
465 suggesting that altered expression of these genes may have influenced cell wall
466 remodeling and sugar partitioning in MIM166 tubers. A recent study showed that
467 suppression of an Ovate Family Protein - *StOFP20* (Soltu.DM.09G010420) caused a
468 shift from round to oval-shaped tubers (Ju *et al*., 2023). In our RNA-seq data, we do
469 not see a marked difference in the *StOFP20* gene expression; however distinct
470 expression patterns of 19 other *OFPs* suggest the involvement of more than one *OFP*
471 gene in influencing tuber shape (Figure S5C). Additionally, several genes from the Ro
472 locus (Fan *et al*., 2022) were downregulated in KD_Head compared to WT_Head
473 (Figure 4F; Table S3). These include a Glycosyl hydrolase (Soltu.DM.10G018520)
474 potentially involved in cell wall remodeling (Barnes and Anderson, 2018), an
475 Aminophospholipid ATPase (Soltu.DM.10G018550) linked to membrane asymmetry

476 and cell expansion (Davis *et al*., 2020), and HSI2-like genes (Soltu.DM.10G018620,
477 Soltu.DM.10G018640), members of the B3 DNA-binding domain family that, in
478 *Arabidopsis*, repress AGL15 via PRC2-mediated H3K27me3 deposition (Chen *et al*.,
479 2018). Taken together, altered phytohormone dynamics and differential expression of
480 genes from the QTL regions, especially the Ro locus and OFPs, likely contributed to
481 the altered tuber shape and radial expansion observed in MIM166 lines. These results
482 raise further questions such as- what molecular factors demarcate the swelling *vs.* sub-
483 swelling boundary during tuber development. Is there a cross talk between miR166-
484 *HD-ZIP III*-phytohormone module and QTL genes?

485 Cyanidin 3-glucoside, pelargonidin 3-glucoside, and delphinidin 3-glucoside
486 are water-soluble anthocyanins with strong antioxidant and anti-inflammatory
487 properties (Noda *et al*., 2002; Duarte *et al*., 2018). In our study, MIM166 tubers
488 showed differential accumulation of these pigments in the peel, but not in their flesh
489 (Figure 6A-B). A similar phenotype was reported in tomato, where overexpression of
490 a petunia chalcone isomerase (CHI) gene increased peel flavonoids by 78-fold
491 without affecting the flesh (Muir *et al*., 2001). In another study, Bovy *et al*. (2002)
492 overexpressed the maize transcription factors LC and C1 in tomato that activated the
493 flavanols pathway, but failed to produce the flavonoids, possibly due to unchanged
494 expression of CHI and flavanone-3′-hydroxylase (F3′H) and flavanone-3′5′-
495 hydroxylase (F3′5′H) genes. In our transcriptomic analysis, we observed an up
496 regulation of multiple structural and accessory genes from the anthocyanin
497 biosynthesis pathway in KD tissues compared to WT, consistent with the increased
498 pigment accumulation (Figure 6C; Figure S7A). Transcription factor families which
499 highly correlated with these pathway genes—bHLH, WRKY, GRAS, bZIP, LBD,
500 ARF, B3, G2-like, HB-other, HD-ZIP, MYB, and MYB-related—also showed
501 significant differential expression (Figure 6D; Table S3–S4; Figure S7A–B). In Apple,
502 degradation of MdIAA121 induced by auxin treatment releases MdARF13, which
503 acts as a negative regulator of the anthocyanin metabolic pathway (Wang *et al*., 2018).
504 Also, auxin inhibits the accumulation of anthocyanin in apple by degrading the
505 MdIAA26 protein (Wang *et al*., 2020). A tuberizing stolon is known to have high
506 auxin at its apex for facilitating tuber development. We speculate this could have
507 restricted pigments accumulation to the tuber peels only in the miR166 KD lines.
508 Conversely, flavonoids may act as inhibitors of auxin transport (Gayomba *et al*., 2016)
509 which might have affected auxin distribution in the KD stolons. Further studies are

510 required to ascertain whether the auxin dynamics in tuberizing stolons and
511 anthocyanin accumulation are inter-linked.
512 Under tuber inductive SD photoperiod, SWEET11b- SP6A interacts to
513 mediate the symplastic loading of sucrose, and prevents its loss to the apoplastic route
514 (Abelenda *et al*., 2019). SWEET11b expression was drastically reduced in all the
515 MIM166 lines (Figure 3G and Figure 4D). Also, the vascular structures in the KD
516 stem were distorted (Figure 2H). The MIM166 plants had reduced tuber yield under
517 SD photoperiod, with no significant changes in the starch content per gram fresh
518 weight of the tuber (Figure 3B and 3F). Thus, the reduced productivity could be due
519 to the altered vascular structure of the stem, reduced symplastic loading of sucrose, or
520 impaired tuber-bulking at the stolon apex due to disrupted phytohormone dynamics.
521 Interestingly, MIM166 plants developed floral buds at the shoot apex and aerial
522 stolon/tubers under SD photoperiod (Figure S12A-C), denoting the formation of
523 ectopic sinks due to the improper sucrose distribution. As SD induction progressed,
524 the belowground developing tubers acted as the primary and stronger sinks, thus
525 limiting sucrose availability for the ectopic sinks.
526
527 **HD-ZIP III TFs are involved in tuberization**
528 Auxin plays a key role in the stolon-to-tuber transition. The stolon apical meristem
529 (StAM) is a major site of auxin biosynthesis, where YUC-like1 (*StYUC4*) acts as a
530 key contributor (Roumeliotis *et al*., 2012). In *Arabidopsis*, REVOLUTA regulates
531 promoters of auxin biosynthesis, transport, and signaling genes (Brandt *et* al., 2012;
532 Reinhart *et al*., 2013). In our study, phenotypes such as impaired root growth,
533 increased tuber sprout branching, and altered auxin-related gene expression suggested
534 a role for REV in potato (Figure 7A–C). Through GUS assay, we observed that the
535 promoter activity of *REV* was visible in the apex of stolons, vascular region and
536 subsequent tuberizing stages (Figure 7D). This was similar to the activity of an auxin
537 responsive promoter, (*DR5:GUS*) observed by Roumeliotis *et al*. (2012), suggesting a
538 putative overlap of *REV* expression and auxin accumulation. REV antisense (REV AS)
539 lines exhibited reduced tuber yield, suggesting a hitherto unknown role of REV in
540 tuberization (Figure 7E-G). The HD-ZIP III binding motif, AT[G/C]AT, was enriched
541 in promoters of potato auxin biosynthesis genes, implying REV-mediated regulation
542 (Figure 7H). Our transient overexpression of *StREV* in the leaves of potato (cv.
543 Désirée) suggests that REV could act as a suppressor of *StYUC4/7/8* expression

544 (Figure 7I) in potato, as opposed to its transcription-activator role in *Arabidopsis*.
545 Auxin levels are dynamic during tuberization, and further studies are needed to clarify
546 the role of REV in regulating auxin during stolon differentiation. Besides REV, other
547 members of the HD-ZIP III family could also play a role in the stolon-to-tuber
548 transitions (Figure S10B). For example, whether HB8 and ICU1/2 are necessary for
549 vascular development of the tuber?

550 Fruit/organ shape is determined during its development. Similar to the
551 findings in tomato and apple (Stembridge and Morrell, 1972; Wang *et al*., 2019; Chen
552 *et al*., 2020), we hypothesize that the tuber shape in potato is governed by
553 phytohormone dynamics (Figure 8). The miR166–HD-ZIP III module is crucial in
554 phytohormone response pathways, and are shown to modulate the expression of each
555 other. In potato stolons, REVOLUTA may act to repress auxin biosynthesis genes
556 (Figure 7), while PHABULOSA, as shown in soybean, could modulate GA
557 metabolism (Figure 8; Zhao *et al*., 2022). Together, these TFs likely coordinate
558 auxin/GA homeostasis in the swelling and sub-swelling stolon, thereby affecting the
559 tuber shape. Additionally, HB8 and INCURVATA are shown to exert antagonistic
560 effects on vascular differentiation in *Arabidopsis* (Kim *et al*., 2005), and auxin
561 positively modulates HB8 expression through ARF5/MONOPTEROS (Donner *et al*.,
562 2009). Development of vascular tissues in differentiating stolon is crucial for delivery
563 of nutrients and photoassimilates. We propose that the miR166–HB8/ICU1/2 likely
564 coordinates vascular differentiation and patterning in developing stolon (Figure 8) and
565 miR166 and its targets- the HD-ZIP III members play multifaceted roles in regulating
566 tuber development.

567 To our knowledge, the role of *miR166-HD-ZIP III* module in storage organ
568 development has not been studied. Here, we demonstrate that miR166 plays
569 conserved roles in regulating numerous developmental processes such as plant height,
570 vascular structure, leaf curvature, and root development, and unique roles in
571 regulating tuber shape, color, and productivity. We also show that REVOLUTA
572 affects tuberization and could regulate the expression of auxin related genes in potato.
573 Further studies are required to explore the roles of miR166 and HD-ZIP III members
574 in tuber tissue patterning and development. In conclusion, our findings establish that
575 miR166 is an important regulatory element in potato, having significant impact on
576 tuber development, morphology, and productivity.
577

578 **Materials and Methods**

579

580 **Plant material and growth conditions**

581 A photoperiod-responsive potato cultivar *Solanum tuberosum* ssp. *andigena* 7540
582 which tuberizes under SD conditions, was used in this study. *In vitro* plants (wild-type
583 and transgenic lines) were propagated from axillary node sub-cultures on Murashige
584 and Skoog's basal medium with 2% (w/v) sucrose (Murashige and Skoog., 1962) and
585 were grown in a plant growth incubator (Percival Scientific, Inc.) with a light
586 intensity of 300 μmol m−2 s−1 under LD conditions unless mentioned otherwise.

587

588 **Prediction and detection of miR166 precursors in potato**

589 Four precursor sequences (stu-MIR166a, stu-MIR166b, stu-MIR166c and stu-
590 MIR166d) of *miR166* were retrieved from the miRBase (http://mirbase.org/; Griffiths-
591 Jones S *et al*., 2008). The secondary structures of these precursors were predicted
592 using the Mfold software (http://www.unafold.org/mfold/applications/rna-folding-
593 form.php; Zuker, 2003), and structures with lowest free energies were then further
594 screened for having the characteristic stem-loop secondary structure with the mature
595 miRNA sequence in the arm region of the stem-loop. All four miRNA precursors
596 were then validated from *S. tuberosum* ssp. *andigena* 7540 by RT-PCR analysis. The
597 sequences of all the oligos used in this study are provided in Table S5, and the IDs for
598 all the genes are in the Table S6.

599 Total RNA was harvested from shoot apex, mature leaves and stolon tissues of
600 potato using RNAiso Plus (DSS TAKARA) as per the manufacturer's instructions.
601 cDNA was synthesized using two microgram (2μg) of total RNA, Superscript IV
602 Reverse Transcriptase (Invitrogen), and oligo dT primers. miRNA precursors were
603 amplified by RT-PCR using precursor-specific primer pairs. The amplicons were
604 cloned into sub-cloning vector pGEMT-easy (Promega) and sequence verified.

605

606 **Validation of mature miR166**

607 Total RNA was isolated using RNAiso Plus (DSS TAKARA) from mature leaves and
608 stolons of WT potato plants. One microgram (1 μg) of total RNA was used for cDNA
609 preparation using miR166 specific stem-loop primers (STP) followed by their end-
610 point PCRs using miR166 specific forward and universal reverse primer as described
611 in Varkonyi-Gasic *et al*. (2007) (Table S5).

612

613 **Tissue-specific relative abundance of miR166 under SD and LD conditions**

614 For investigating the influence of photoperiod on tissue-specific accumulation of
615 mature *miR166*, *in vitro* grown wild-type *S. tuberosum* spp. *andigena* 7540 plants
616 were transferred to soil and maintained under LD photoperiod with 300 μmol m−2
617 s−1 light intensity for a period of ten weeks (until they attained 10-12 leaf stages) in a
618 growth chamber (Percival Scientific, Inc.). Later, half of the plants were transferred to
619 tuber-inductive SD photoperiod for 7 days, while the remaining plants were
620 maintained under LD conditions. Leaves and stages of stolon-to-tuber transitions were
621 collected at 7 days post LD/SD induction in triplicates. Isolation of total RNA and
622 cDNA synthesis was carried out as described before. qPCR reactions were performed
623 on CFX96 Real-Time System (BIO-RAD) with miR166-specific forward primer and
624 universal reverse primer, using TAKARA SYBR green master mix (Takara-Clontech).
625 The reaction mix was incubated at 95 °C for 30 s, followed by 40 cycles at 95 °C for
626 5 s, gene-specific annealing temperature for 15 s and extension for 72 °C for 15 s.
627 PCR specificity was checked by melting curve analysis, and data were analyzed using
628 the $2^{-\Delta\Delta Ct}$ method (Livak and Schmittgen, 2001).

629

630 **Generation of constructs and potato transgenic lines**

631 MicroRNA166 overexpression (OE) and mimicry (MIM) constructs for
632 overexpression and suppression of the miR166, respectively, were previously
633 generated in our lab. Briefly, miR166 OE construct- 35S:St-pre166D-pBI121 was
634 generated by amplifying precursor (St-pre166-d) from potato RNA using primers
635 Pre166d-FP and Pre166d-RP (Table S5). The amplified product (108 bp) was cloned
636 into the binary vector pBI121 downstream to the 35S CaMV constitutive promoter.
637 For knockdown (KD) construct, we used artificial target mimicry (MIM) strategy.
638 The KD construct (originally in pGREEN vector) was obtained from European
639 *Arabidopsis* Stock Centre (NASC) (Todesco *et al*., 2010), and the MIM166 insert
640 (542 bp) was re-cloned to pBI121 binary vector to generate 35S:MIM166-pBI121.
641 Both these constructs- OE and MIM were then mobilized into *Agrobacterium*
642 *tumefaciens* strain GV3101. Transgenic potato plants in *S. tuberosum* spp. *andigena*
643 7540 were generated as described in Banerjee *et al*., 2006. Kanamycin-resistant
644 transgenic plants were further screened by molecular methods and selective lines were
645 used for further experiments.

646 After 4 weeks of *in vitro* growth, potato plants were transferred to soil, grown
647 for 7-9 weeks under LD conditions, before initiating SD induction. Phenotypic
648 characteristics such as plant height, number of nodes and leaf curvature were recorded
649 just before the initiation of SD photoperiod treatment, whereas the frequency of floral
650 bud formation and tuber productivity parameters were measured after 1 and 8-9 weeks
651 of SD induction, respectively.
652
653 **Phenotypic analysis**
654 All the phenotypic analyses were performed on 6–7 weeks old soil-grown plants.
655 Shoot height was measured from the bottom-most node up to the plant apex. For
656 measurement of leaf curvature indices, mature terminal leaves at the fifth node were
657 analyzed as described in Liu *et al*., 2010. These experiments were performed at least
658 three times with similar results.
659
660 **Assessment of tuber productivity**
661 One-month-old plantlets of the transgenic lines and WT were transferred to soil in
662 small round pots and hardened for one week under LD conditions in a growth
663 chamber (Percival Scientific, Inc.) with a light intensity of 300 μmol m−2 s−1, day
664 temperature of 24°C, and night temperature of 22°C. This was followed by an
665 additional three weeks of incubation in the same pots. Subsequently, the plants were
666 re-potted into medium-sized pots and continued to grow under LD conditions for an
667 additional five weeks. When the plants reached the 10-12 leaf stage, they were
668 transferred to tuber inductive short-day (SD) conditions (16h dark and 8h light) with
669 day and night temperatures of 22°C and 20°C, respectively. A subset of these plants
670 was harvested after 7 days of induction, and stolons were collected for RT-qPCR
671 analysis. After 60 days of induction, remaining plants were evaluated for their tuber
672 productivity (gram fresh weight [g fr wt] per plant) and tuber numbers. This
673 experiment was carried out 3 times, with consistent results. For tuber sphericity index
674 and volume assessment, 30 tubers per line were measured for their diameters
675 (Diameter1, Diameter2 and height). *In vitro* tuber induction assay was performed
676 (experiment was repeated three times independently) as described in Kondhare *et al*.,
677 2021.
678
679 **Starch estimation**

680 Starch estimation was carried out twice, independently, as described in Kamble *et al*.
681 (2023), Hawkins *et al*. (2021) and Kringel *et al*. (2020), with minor modifications.
682 Tuber tissue was well-homogenized in cold water containing 0.35% sodium
683 metabisulphte. The slurry was filtered to remove the debris. Filtered solution was kept
684 undisturbed for 1 hour at 4 degrees. Insoluble material was collected by centrifugation,
685 followed by 3 washes with 80% ethanol, and then finally re-suspended in water.
686 Starch was digested using alpha amylase (SRL), glucoamylase (SRL) and
687 Amyloglucosidase (Sigma). Glucose was estimated using the DNSA method, and
688 compared with a standard graph prepared using Starch (Sigma), digested under
689 identical conditions.
690
691 **RNA sequencing**
692 For RNA-sequencing, miR166 KD #3 and WT plants were grown in soil for 10-weeks
693 under LD conditions and subjected to SD induction for 12 days. Swollen stolons were
694 harvested in triplicates (from at least 20 plants per replicate) and divided into swelling
695 (Head) and sub-swelling region (SSR) and snap-frozen in liquid nitrogen. The tissues
696 were crushed using liquid Nitrogen and stored in -80º C until further use. For RNA
697 sequencing and RT-qPCR purposes, 100 mg of tissue from each sample was used to
698 isolate the total RNA using RNAiso Plus as per the manufacturer's instructions. RNA
699 quality and integrity were assessed, and RNA-sequencing was performed by
700 Novelgene Technologies Pvt. Ltd., Hyderabad. Paired-end sequencing was performed
701 on Illumina NovaSeq 6000, adapter sequences and low-quality reads were filtered
702 using FASTP to get high-quality reads on the parameter of <Q20, length < 50. Further
703 processing was performed as described in Kumar *et al*. 2020. Validation of selected
704 target genes identified in the RNA-seq analysis was done using qPCR as described
705 above.
706
707 **Detection of phytohormones and pigments by LC-MS/MS**
708 Tissues- stolon, swollen stolon (Head and SSR), tuber peel, tuber flesh were harvested,
709 crushed in liquid Nitrogen, and stored at -80º C until further use. 100 mg of the
710 crushed powder was extracted with 1 ml of extraction solvent (For phytohormone
711 extraction- MS grade methanol/water/formic acid 75:20:5; having 300ng internal
712 standard Adonitol; For pigment extraction- 80 percent methanol in MS grade water;
713 having 300ng internal standard Adonitol), by 3-5 min of vigorous vortex, followed by

714 15 min of sonication. The solution was incubated overnight at -80°C under dark
715 conditions. Next day, the samples were centrifuged at 4°C, maximum speed for 15
716 min. The supernatant was transferred into a new tube, and reduced to half of its
717 original volume, using centrivap at 4°C, and was filtered through 0.22-micron syringe
718 filter. The LC-MS system (Exion AD, AB Sciex) was used for detection of
719 phytohormones and pigments. Chromatographic separation was done on AB SCIEX
720 Exion LC AD UPLC system, using Phenomenex kinetex core shell C18 column
721 (2.1X150 mm, 1.7µm). Separation of compounds was performed at 0.3 ml/ min flow
722 rate with linear gradient of solvent A (milliQ + 0.1% formic acid) and solvent B
723 (Acetonitrile + 0.1% formic acid) was performed as follows: 0 min 5% B + 95% A; 3
724 min, 10% B; 6 min, 50% B, 7 min, 70% B; 10 min, 95% B; 12 min, finally column
725 was re-equilibrated to initial ratio of 5% B + 95% A for 4 min with total run time of
726 16 min. The m/z range for phytohormone and pigment detection was 100-400 and
727 100-1700, respectively. The sample injection volume was 40 µl for all the samples.
728 Three blank runs were given every time between the biological replicates throughout
729 run. The full scan mass spectrometry data was acquired on the X500R Q-TOF (AB
730 Sciex, USA). The data for all the samples were acquired using electrospray ionization
731 in both positive and negative modes. Mass calibration was performed in positive and
732 negative ion modes before the data acquisition. Data analysis was carried out using
733 the SCIEX OX software provided along with the machine.
734
735 **GUS assay**
736 *StREV* promoter transgenic lines (promREV:*uidA*) were grown *in vitro* under LD
737 conditions for 20 d. They were also grown in soil under LD conditions for 8 weeks,
738 followed by SD induction for 15 d. Entire *in vitro* grown plantlets, stolon and tuber
739 samples from SD-induced soil-grown plants were subjected to GUS assay as
740 described in Begum *et al*., (2022) and imaged using olympus MX stereozoom
741 microscope.
742
743 **Chlorophyll and anthocyanin estimation**
744 Anthocyanin and chlorophyll estimation from leaves of WT and miR166 KD lines
745 was performed as per the method in Nakata and Ohme-Takagi (2014) and
746 Bhattacharjee and Sharma (2012), respectively. These experiments were conducted
747 two times, with similar results.

748

749 **Histology**

750 For anatomical studies, stems from the middle part of soil-grown plants (6 weeks LD)
751 were used. Free hand transverse sections were cut using a sharp razor blade, and
752 selective sections were stained with Toluidine Blue O solution as described in
753 Pradhan Mitra and Loqué., 2014. The sections were mounted in 70% glycerol, before
754 imaging them on the Nikon Eclipse microscope.

755

756 **Infiltration assay**

757 *Agrobacterium*-mediated co-infiltration assay was performed in leaves of 6-week old
758 WT potato (cv. *Désirée*). *35S:StREV* cloned in pCB201 construct was transformed
759 into *A. tumefaciens* GV3101 strain. An overnight grown primary culture was used to
760 inoculate 100 ml secondary culture (having 150 µM acetosyringone) without any
761 antibiotics. When the secondary culture reached an OD600 of 1.00, it was centrifuged,
762 and the cell pellet was resuspended in the infiltration buffer (10 mM MgCl2, 10 mM
763 MES-K: pH= 5.6, plus 150 µM acetosyringone), incubated at RT on a tube-roller for
764 at least 3 hrs, followed by infiltration into the leaves of potato plants using a
765 needleless syringe. Infiltration with only the infiltration buffer served as experimental
766 control. Leaves were harvested 72 hrs post-infiltration, and subjected further for RNA
767 isolation and RT-qPCR analyses. This experiment was conducted three times with
768 similar results.

769

770 **Data availability**

771 The raw sequencing data were deposited in the NCBI Short Read Archive (SRA)
772 database (http://www.ncbi.nlm.nih. gov/sra/). It can be retrieved using the SRA ID
773 SRP630954. All other relevant data can be found within the manuscript and its
774 supporting materials.

775

776 **Acknowledgements**

777 Authors acknowledge Mr. Nilesh Lohakare and Mr. Nitish Lahigude (Indian Institute
778 of Science Education and Research, Pune) for their help in maintaining the plants in
779 the green house facility. We thank Novelgene Technologies Pvt. Ltd. for performing
780 RNA sequencing. We are thankful to Dr. Harpreet Singh Kalsi, Dr. Nilam Malankar,
781 Dr. Kirtikumar Kondhare and Ms. Shikha Singh for their inputs.

**Funding**

NSP and JK are thankful to the University Grants Commission for the Senior Research Fellowship and Junior Research Fellowship, respectively. GA acknowledges funding received from the Department of Biotechnology, India. AKB acknowledges the support and generous funding from the Indian Institute of Science Education and Research (IISER) Pune.

**Authors contributions**

N.S.P. designed the experiments, generated transgenic lines, carried out phenotypic and transcriptomic data analyses, conducted experiments and wrote the manuscript draft. A.V. conducted the LC-MS/MS experiments and analyzed its data. J.K. carried out the infiltration experiment and performed its molecular analysis. G.A. and N.S.P. generated the miR166 KD and promREV::uidA transgenic lines. B.N. and N.S.P. performed RLM-RACE for target validation. A.K.B. supervised the study, obtained the funding and resources. N.S.P. and A.K.B. conceived the idea and edited the manuscript. All authors have read and approved the final manuscript.

**Conflict of Interest Statement**

The authors declare that they have no conflicts of interest associated with this work.

**Ethics Statement**

All experimental research on plants in this study complied with institutional bio-safety guidelines. The plant materials used were maintained in accordance with relevant regulations.

**Supporting Information**

**Figure S1.** Details of the precursors and mature miR166 in potato

**Figure S2.** Abundance of *miR166* in stolons under early LD vs SD stages from a photoperiod dependent tuberizing variety ssp. *andigena* 7540

**Figure S3.** Pleiotropic phenotypes of miR166 suppression on potato

**Figure S4.** PCA and Volcano plots of samples processed for RNA-sequencing

**Figure S5.** Heatmap for selective genes from the QTLs

816 **Figure S6.** Heat maps for phytohormone genes and tuber sprouts phenotype of
817 miR166 KD lines
818 **Figure S7.** Heat map for anthocyanin biosynthesis pathway genes and TF families
819 **Figure S8.** Characterization of the miR166 OE lines
820 **Figure S9.** Characterization of the REV AS lines
821 **Figure S10.** Relative fold change of the *HD-ZIP class III* transcripts
822 **Figure S11.** GA8 quantification from *in vitro* miR166 KD plants
823 **Figure S12.** Development of ectopic sinks in miR166 KD lines under SD photoperiod
824
825 **Supporting Tables**
826 **Table S1.** Differentially expressed genes in WT_Head compared to WT_SSR
827 **Table S2.** Differentially expressed genes in KD_Head compared to KD_SSR
828 **Table S3.** Differentially expressed genes in KD_Head compared to WT_Head
829 **Table S4.** Differentially expressed genes in KD_SSR compared to WT_SSR
830 **TableS5.** List of Primers
831 **Table S6.** List of gene IDs
832
833 **Supporting Data S1.** MS-MS fragment match for phytohormones and pigments
834
835 **References**


836 • Abelenda JA, Bergonzi S, Oortwijn M, Sonnewald S, Du M, Visser RGF,
837 Sonnewald U, Bachem CWB. 2019. Source-sink regulation is mediated by
838 interaction of an FT homolog with a SWEET protein in potato. Curr Biol.
839 29:1178–1186.e6. doi:10.1016/j.cub.2019.02.018
840 • Baima S, Possenti M, Matteucci A, Wisman E, Altamura MM, Ruberti I,
841 Morelli G. 2001. The Arabidopsis ATHB-8 HD-Zip protein acts as a
842 differentiation-promoting transcription factor of the vascular meristems. Plant
843 Physiol.
844 • Banerjee AK, Prat S, Hannapel DJ. 2006. Efficient production of transgenic
845 potato (S. tuberosum L. ssp. andigena) plants via Agrobacterium tumefaciens-
846 mediated transformation. Plant Sci. 170:732–738.
847 doi:10.1016/j.plantsci.2005.11.007

848 • Barnes, W. J., & Anderson, C. T. (2018). Release, recycle, rebuild: Cell-wall
849 remodeling, autodegradation, and sugar salvage for new wall biosynthesis
850 during plant development. Molecular Plant, 11(1), 31–46.
851 https://doi.org/10.1016/j.molp.2017.08.011
852 • Begum S, Jing S, Yu L, Sun X, Wang E, Abu Kawochar M, Qin J, Liu J, Song
853 B. 2022. Modulation of JA signalling reveals the influence of StJAZ1-like on
854 tuber initiation and tuber bulking in potato. Plant J. 109:952–964.
855 doi:10.1111/tpj.15606
856 • Bhattacharjee S, Sharma GD. 2012. Effect of dual inoculation of arbuscular
857 mycorrhiza and rhizobium on the chlorophyll, nitrogen and phosphorus
858 contents of pigeon pea (Cajanus cajan L.). Adv Microb. 2:25945.
859 doi:10.4236/aim.2012.24072
860 • Bhogale S, Mahajan AS, Natarajan B, Rajabhoj M, Thulasiram HV, Banerjee
861 AK. 2014. MicroRNA156: a potential graft-transmissible microRNA that
862 modulates plant architecture and tuberization in Solanum tuberosum ssp.
863 Andigena. Plant Physiol. 164:1011–1027.
864 • Boualem A, Laporte P, Jovanovic M, Laffont C, Plet J, Combier JP, Niebel A,
865 Crespi M, Frugier F. 2008. MicroRNA166 controls root and nodule
866 development in Medicago truncatula. Plant J. 54:876–887. doi:10.1111/j.1365-
867 313X.2008.03448.x
868 • Brandt R, Salla-Martret M, Bou-Torrent J, Musielak T, Stahl M, Lanz C, Ott F,
869 Schmid M, Greb T, Schwarz M, Choi SB, Barton MK, Reinhart BJ, Liu T,
870 Quint M, Palauqui JC, Martínez-García JF, Wenkel S. 2012. Genome-wide
871 binding-site analysis of REVOLUTA reveals a link between leaf patterning
872 and light-mediated growth responses. Plant J. 72:31–42. doi:10.1111/j.1365-
873 313X.2012.05049.x
874 • Bovy A, Schijlen E, Hall RD (2007) Metabolic engineering of flavonoids in
875 tomato (Solanum lycopersicum): the potential for metabolomics.
876 Metabolomics 3: 399–412. https://doi.org/10.1007/s11306-007-0074-2
877 • Chen H, Rosin FM, Prat S, Hannapel DJ. 2003. Interacting transcription
878 factors from the three-amino acid loop extension superclass regulate tuber
879 formation. Plant Physiol. 132:1391–1404. doi:10.1104/pp.103.022434

880 • Chen S, Wang XJ, Tan GF, Zhou WQ, Wang GL. 2020. Gibberellin and the
881 plant growth retardant paclobutrazol altered fruit shape and ripening in tomato.
882 Protoplasma. 257:853–861. doi:10.1007/s00709-019-01471-2
883 • Chen X, Yao Q, Gao X, Jiang C, Harberd NP, Fu X. 2016. Shoot-to-root
884 mobile transcription factor HY5 coordinates plant carbon and nitrogen
885 acquisition. Curr Biol. 26:640–646.
886 • Chen, N., et al. (2018). HSI2/VAL1 silences AGL15 to regulate the
887 developmental transition from seed maturation to vegetative growth in
888 Arabidopsis. The Plant Cell, 30(3), 600–619.
889 https://doi.org/10.1105/tpc.17.00893
890 • Clepet C, Devani RS, Boumlik R, Hao Y, Morin H, Marcel F, Verdenaud M,
891 Mania B, Brisou G, Citerne S, Mouille G, Lepeltier JC, Koussevitzky S,
892 Boualem A, Bendahmane A. 2021. The miR166–SlHB15A regulatory module
893 controls ovule development and parthenocarpic fruit set under adverse
894 temperatures in tomato. Mol Plant. 14:1185–1198.
895 doi:10.1016/j.molp.2021.05.005
896 • Davis, J. A., Pares, R. B., Bernstein, T., McDowell, S. C., Brown, E., Stubrich,
897 J., et al. (2020). The lipid flippases ALA4 and ALA5 play critical roles in cell
898 expansion and plant growth. Plant Physiology, 182(4), 2111–2125.
899 https://doi.org/10.1104/pp.19.01332
900 • Ding Y, Gong S, Wang Y, Wang F, Bao H, Sun J, Cai C, Yi K, Chen Z, Zhu
901 C. 2018. MicroRNA166 modulates cadmium tolerance and accumulation in
902 rice. Plant Physiol. 177:1691–1703. doi:10.1104/pp.18.00485
903 • Donner, T. J., Sherr, I., & Scarpella, E. (2009). Regulation of preprocambial
904 cell state acquisition by auxin signaling in Arabidopsis leaves. Development,
905 136(19), 3235-3246. https://doi.org/10.1242/dev.037028
906 • Draffehn AM, Meller S, Li L, Gebhardt C. 2010. Natural diversity of potato
907 (Solanum tuberosum) invertases. BMC Plant Biol. 10:271. doi:10.1186/1471-
908 2229-10-271
909 • Duarte LJ, Chaves VC, Nascimento MVP dos S, Calvete E, Li M, Ciraolo E,
910 Ghigo A, Hirsch E, Simões CMO, Reginatto FH, Dalmarco EM. 2018.
911 Molecular mechanism of action of pelargonidin-3-O-glucoside, the main

912 anthocyanin responsible for the anti-inflammatory effect of strawberry fruits.
913 Food Chem. 247:56–65. doi:10.1016/j.foodchem.2017.12.015

- 914 Fan G, Wang Q, Xu J, Chen N, Zhu W, Duan S, Yang X, De Jong WS, Guo Y,
915 Jin L, Li G. 2022. Fine mapping and candidate gene prediction of tuber shape
916 controlling Ro locus based on integrating genetic and transcriptomic analyses
917 in potato. Int J Mol Sci. 23:1470. doi:10.3390/ijms23031470
- 918 Gayomba, S. R., Watkins, J. M., & Muday, G. K. (2016). Flavonols regulate
919 plant growth and development through regulation of auxin transport and
920 cellular redox status. In K. Yoshida, V. Cheynier, & S. Quideau (Eds.), Recent
921 Advances in Polyphenol Research (Vol. 5, pp. 143–170). John Wiley & Sons.
922 https://doi.org/10.1002/9781118883303.ch7
- 923 Griffiths-Jones S, Saini HK, van Dongen S, Enright AJ. 2008. miRBase: tools
924 for microRNA genomics. Nucleic Acids Res. 36:D154–D158.
- 925 Hannapel DJ, Sharma P, Lin T, Banerjee AK. 2017. The multiple signals that
926 control tuber formation. Plant Physiol. 174:845–856.
- 927 Hawkins E, Chen J, Watson-Lazowski A, Ahn-Jarvis J, Barclay JE, Fahy B,
928 Hartley M, Warren FJ, Seung D. 2021. STARCH SYNTHASE 4 is required
929 for normal starch granule initiation in amyloplasts of wheat endosperm. New
930 Phytol. 230:2371–2386. doi:10.1111/nph.17342
- 931 Jia X, Ding N, Fan W, Yan J, Gu Y, Tang X, Li R, Tang G. 2015. Functional
932 plasticity of miR165/166 in plant development revealed by small tandem
933 target mimic. Plant Sci. 233:11–21. doi:10.1016/j.plantsci.2014.12.020
- 934 Ju A, Wang Y, Yan Y, Li C, Luo W, Ma L, Shang Y, Gao D. 2023. StOFP20
935 regulates tuber shape and interacts with TONNEAU1 recruiting motif proteins
936 in potato. J Integr Agric. 22:752–761. doi:10.1016/j.jia.2022.08.069
- 937 Kamble UN, Makhamadjonov F, Fahy B, Martins C, Saalbach G, Seung D.
938 2023. Initiation of B-type starch granules in wheat endosperm requires the
939 plastidial α-glucan phosphorylase PHS1. Plant Cell. 35:4091–4110.
940 doi:10.1093/plcell/koad217
- 941 Kim J, Jung JH, Reyes JL, Kim YS, Kim SY, Chung KS, Kim JA, Lee M, Lee
942 Y, Kim VN, Chua NH, Park CM. 2005. microRNA-directed cleavage of
943 ATHB15 mRNA regulates vascular development in Arabidopsis inflorescence
944 stems. Plant J. 42:84–94. doi:10.1111/j.1365-313X.2005.02354.x

945 • Kondhare KR, Kumar A, Patil NS, Malankar N, Saha K, Banerjee AK. 2021.
946 Development of aerial and belowground tubers in potato is governed by
947 photoperiod and epigenetic mechanism. Plant Physiol. 187:1071–1086.
948 doi:10.1093/plphys/kiab409
949 • Kondhare KR, Malankar NN, Devani RS, Banerjee AK. 2018. Genome-wide
950 transcriptome analysis reveals small RNA profiles involved in early stages of
951 stolon-to-tuber transitions in potato under photoperiodic conditions. 1–19.
952 • Kringel DH, el Halal SLM, Zavareze Eda R, Dias ARG. 2020. Methods for
953 the extraction of roots, tubers, pulses, pseudocereals, and other unconventional
954 starch sources: a review. Starch/Staerke. 72:11–12.
955 doi:10.1002/star.201900234
956 • Kumar A, Kondhare KR, Vetal PV, Banerjee AK. 2020. PcG proteins MSI1
957 and BMI1 function upstream of miR156 to regulate aerial tuber formation in
958 potato. Plant Physiol. 182:185–203. doi:10.1104/pp.19.00416
959 • Lakhotia N, Joshi G, Bhardwaj AR, Katiyar-Agarwal S, Agarwal M,
960 Jagannath A, Goel S, Kumar A. 2014. Identification and characterization of
961 miRNAome in root, stem, leaf and tuber developmental stages of potato
962 (Solanum tuberosum L.) by high-throughput sequencing. BMC Plant Biol.
963 14:6.
964 • Li N, Yang T, Guo Z, Wang Q, Chai M, Wu M, Li X, Li W, Li G, Tang J,
965 Tang G, Zhang Z. 2020. Maize microRNA166 inactivation confers plant
966 development and abiotic stress resistance. Int J Mol Sci. 21:9506.
967 doi:10.3390/ijms21249506
968 • Lin Y, Liu T, Liu J, Liu X, Ou Y, Zhang H, Li M, Sonnewald U, Song B, Xie
969 C. 2015. Subtle regulation of potato acid invertase activity by a protein
970 complex of invertase, invertase inhibitor, and sucrose nonfermenting1-related
971 protein kinase. Plant Physiol. 168(4):1807–1819. doi:10.1104/pp.15.00664
972 • Lindqvist-Kreuze H, Khan A, Salas E, Meiyalaghan S, Thomson S, Gomez R,
973 Bonierbale M. 2015. Tuber shape and eye depth variation in a diploid family
974 of Andean potatoes. BMC Genet. 16:57. doi:10.1186/s12863-015-0213-0
975 • Liu Z, Jia L, Mao Y, He Y. 2010. Classification and quantification of leaf
976 curvature. J Exp Bot. 61:2757–2767. doi:10.1093/jxb/erq111

977 • Livak KJ, Schmittgen TD. 2001. Analysis of relative gene expression data
978 using real-time quantitative PCR and the 2(-ΔΔC(T)) method. Methods.
979 25:402–408.
980 • Malankar NN, Kondhare KR, Saha K, Mantri M, Banerjee AK. 2023. The
981 phased short-interfering RNA siRD29(-) regulates GIBBERELLIN 3-
982 OXIDASE 3 during stolon-to-tuber transitions in potato. Plant Physiol.
983 193:2555–2572. doi:10.1093/plphys/kiad493
984 • Martin A, Adam H, Díaz-Mendoza M, Zurczak M, González-Schain ND,
985 Suárez-López P. 2009. Graft-transmissible induction of potato tuberization by
986 the microRNA miR172. Development. 136:2873–2881.
987 • Mingo-Castel AM, Young RE, Smith OE. 1976. Kinetin-induced tuberization
988 of potato in vitro: on the mode of action of kinetin. Plant Cell Physiol. 17:557–
989 567.
990 • Muir S, Collins G, Robinson S, et al. 2001. Overexpression of petunia
991 chalcone isomerase in tomato results in fruit containing increased levels of
992 flavonols. Nat Biotechnol. 19:470–474. doi:10.1038/88150
993 • Murashige T, Skoog F. 1962. A revised medium for rapid growth and
994 bioassays with tobacco tissue cultures. Physiol Plant. 15:473–497.
995 doi:10.1111/j.1399-3054.1962.tb08052.x
996 • Nakata M, Ohme-Takagi M. 2014. Quantification of anthocyanin content.
997 Bio-Protoc. 4:1428–1440. doi:10.21769/BioProtoc.1098
998 • Noda Y, Kaneyuki T, Mori A, Packer L. 2002. Antioxidant activities of
999 pomegranate fruit extract and its anthocyanidins: delphinidin, cyanidin, and
1000 pelargonidin. J Agric Food Chem. 50:166–171. doi:10.1021/jf0108765
1001 • Pradhan Mitra P, Loqué D. 2014. Histochemical staining of Arabidopsis
1002 thaliana secondary cell wall elements. J Vis Exp. 87:51381.
1003 doi:10.3791/51381
1004 • Prigge MJ, Otsuga D, Alonso JM, Ecker JR, Drews GN, Clark SE 2005 Class
1005 III homeodomain-leucine zipper gene family members have overlapping,
1006 antagonistic, and distinct roles in Arabidopsis development. Plant Cell 17: 61–
1007 76. https://doi.org/10.1105/tpc.104.026161

1008 • Ramachandran P, Carlsbecker A, Etchells JP. 2017. Class III HD-ZIPs govern
1009 vascular cell fate: an HD view on patterning and differentiation. Physiol Plant.
1010 68:55–69.
1011 • Ross ARS, Vrebalov J, Lang L, Allan WL, Abrams SR, Hall M, Tanksley SD,
1012 van den Berg L, McCourt P. 2010. Potato tuber pectin structure is influenced
1013 by pectin methyl esterase activity and impacts on cooked potato texture. J Exp
1014 Bot. 62(1):371–381. doi:10.1093/jxb/erq280
1015 • Roodbarkelari F, Groot EP. 2017. Regulatory function of homeodomain-
1016 leucine zipper (HD-ZIP) family proteins during embryogenesis. New Phytol.
1017 213:95–104.
1018 • Roumeliotis E, Kloosterman B, Oortwijn M, Kohlen W, Bouwmeester HJ,
1019 Visser RGF, Bachem CWB. 2012. The effects of auxin and strigolactones on
1020 tuber initiation and stolon architecture in potato. J Exp Bot. 63:4539–4547.
1021 doi:10.1093/jxb/ers132
1022 • Sakuraba Y, Yanagisawa S. 2018. Light signalling-induced regulation of
1023 nutrient acquisition and utilisation in plants. Semin Cell Dev Biol. 83:123–132.
1024 doi:10.1016/j.semcdb.2017.12.014
1025 • Sattelmacher B, Marschner H. 1978. Cytokinin activity in stolons and tubers
1026 of Solanum tuberosum during the period of tuberization. Z Pflanzenernähr
1027 Bodenkd. 44.
1028 • Sessa G, Steindler C, Morelli G, Ruberti I. 1998. The Arabidopsis Athb-8, -9
1029 and -14 genes are members of a small gene family coding for highly related
1030 HD-ZIP proteins. Plant Mol Biol. 38.
1031 • Singh A, Singh S, Panigrahi KCS, Reski R, Sarkar AK. 2014. Balanced
1032 activity of microRNA166/165 and its target transcripts from the class III
1033 homeodomain-leucine zipper family regulates root growth in Arabidopsis
1034 thaliana. Plant Cell Rep. 33:945–953. doi:10.1007/s00299-014-1573-z
1035 • Stembridge GE, Morrell G. 1972. Effect of gibberellins and 6-benzyladenine
1036 on the shape and fruit set of 'Delicious' apples. J Am Soc Hort Sci. 97:464–
1037 467.
1038 • Tang D, Jia Y, Zhang J, Li H, Cheng L, Wang P, Bao Z, Liu Z, Feng S, Zhu X,
1039 et al. 2022. Genome evolution and diversity of wild and cultivated potatoes.
1040 Nature. 606:535–541.

1041 • Todesco M, Rubio-Somoza I, Paz-Ares J, Weigel D. 2010. A collection of
1042 target mimics for comprehensive analysis of microRNA function in
1043 Arabidopsis thaliana. PLoS Genet. 6:e1001031.
1044 doi:10.1371/journal.pgen.1001031
1045 • Turchi L, Baima S, Morelli G, Ruberti I. 2015. Interplay of HD-Zip II and III
1046 transcription factors in auxin-regulated plant development. J Exp Bot.
1047 66:5043–5053.
1048 • Valiollahi E, Farsi M, Kakhki AM. 2014. Sly-miR166 and Sly-miR319 are
1049 components of the cold stress response in Solanum lycopersicum. Plant
1050 Biotechnol Rep. 8:349–356. doi:10.1007/s11816-014-0326-3
1051 • Varkonyi-Gasic E, Wu R, Wood M, Walton EF, Hellens RP. 2007. Protocol: a
1052 highly sensitive RT-PCR method for detection and quantification of
1053 microRNAs. Plant Methods. 3:12. doi:10.1186/1746-4811-3-12
1054 • Wang CK, Han PL, Zhao YW, Ji XL, Yu JQ, You CX, Hu DG, Hao YJ. 2020.
1055 Auxin regulates anthocyanin biosynthesis through the auxin repressor protein
1056 MdIAA26. Biochem Biophys Res Commun. 533:717–722.
1057 doi:10.1016/j.bbrc.2020.09.065
1058 • Wang D, Wang S, Zhang D, Meng Y, Qian Y, Feng S, Bai Y, Zhou Y. 2025.
1059 Identification and expression analysis of miR166 gene family in response to
1060 salt stress in Chrysanthemum. Horticulturae. 11:141.
1061 doi:10.3390/horticulturae11020141
1062 • Wang N, Xu HF, Jiang SH, Fang HC, Su MY, Zhang ZY, Zhang TL, Chen
1063 XS. 2018. Auxin regulates anthocyanin biosynthesis through the Aux/IAA–
1064 ARF signaling pathway in apple. Hortic Res. 5:59. doi:10.1038/s41438-018-
1065 0068-4
1066 • Wang Y, Clevenger JP, Illa-Berenguer E, Meulia T, van der Knaap E, Sun L.
1067 2019. A comparison of sun, ovate, fs8.1 and auxin application on tomato fruit
1068 shape and gene expression. Plant Cell Physiol. 60:1067–1081.
1069 doi:10.1093/pcp/pcz024
1070 • Wei X, Wang C, Wang Y, Zhao Y, Ma Y, Liu S, Guan S, Jiao P. 2025.
1071 miR166e/ZmATHB14 module contributes to drought tolerance in maize root.
1072 Int J Biol Macromol. 297:139707. doi:10.1016/j.ijbiomac.2025.139707

1073 • Yadav A, Kumar S, Verma R, Lata C, Sanyal I, Rai SP. 2021. MicroRNA166:
1074 an evolutionarily conserved stress biomarker in land plants targeting HD-ZIP
1075 family. Physiol Mol Biol Plants. 27:2471–2485. doi:10.1007/s12298-021-
1076 01096-x
1077 • Zhang CH, Zhang BB, Ma RJ, Yu ML, Guo SL, Guo L. 2015. Isolation and
1078 expression analysis of four HD-ZIP III family genes targeted by
1079 microRNA166 in peach. Genet Mol Res. 14:14151–14161.
1080 doi:10.4238/2015.October.29.37
1081 • Zhang J, Zhang H, Srivastava AK, Pan Y, Bai J, Fang J, Shi H, Zhu JK. 2018.
1082 Knockdown of rice microRNA166 confers drought resistance by causing leaf
1083 rolling and altering stem xylem development. Plant Physiol. 176:2082–2094.
1084 doi:10.1104/pp.17.01432
1085 • Zhang Y, Pu Y, Zhang Y, Li K, Bai S, Wang J, Xu M, Liu S, Zhou Z, Wu Y,
1086 Hu R, Wu Q, Kear P, Du M, Qi J. 2024. Tuber transcriptome analysis reveals
1087 a novel WRKY transcription factor StWRKY70 potentially involved in potato
1088 pigmentation. Plant Physiol Biochem. 213:108792.
1089 doi:10.1016/j.plaphy.2024.108792
1090 • Zhao C, Ma J, Zhang Y, Yang S, Feng X, Yan J. 2022. The miR166-mediated
1091 regulatory module controls plant height by regulating gibberellic acid
1092 biosynthesis and catabolism in soybean. J Integr Plant Biol. 64:995–1006.
1093 doi:10.1111/jipb.13253
1094 • Zhou C, Yang N, Tian C, Wen S, Zhang C, Zheng A, Hu X, Fang J, Zhang Z,
1095 Lai Z, Lin Y, Guo Y. 2024. The miR166 targets CsHDZ3 genes to negatively
1096 regulate drought tolerance in tea plant (Camellia sinensis). Int J Biol
1097 Macromol. 264:130735. doi:10.1016/j.ijbiomac.2024.130735
1098 • Zhou GK, Kubo M, Zhong R, Demura T, Ye ZH. 2007. Overexpression of
1099 miR165 affects apical meristem formation, organ polarity establishment and
1100 vascular development in Arabidopsis. Plant Cell Physiol. 48:391–404.
1101 doi:10.1093/pcp/pcm008
1102 • Zuker M. 2003. Mfold web server for nucleic acid folding and hybridization
1103 prediction. Nucleic Acids Res. 31:3406–3415.
1104
1105

1106 **Figure legends**

1107 **Figure 1. Identification, Validation, and Expression Analysis of miR166 in Potato**
1108 (A) RT-PCR of miR166 precursors from shoot apex, leaves and stolons tissues of SD
1109 grown *Solanum tuberosum* ssp. *andigena*. (B-D) Quantification of precursor-a, -b, and
1110 -c levels from stolon-to-tuber transition stages (stolon, swollen stolon and mini-tuber)
1111 harvested from potato plants post 10 days of SD or LD induction. Relative transcript
1112 abundance of the gene expression in SD tissue is compared to LD stolons. Asterisks
1113 (one, two, three, and four) indicate significant differences at $p < 0.05$, $p < 0.01$,
1114 $p < 0.001$, and $p < 0.0001$, respectively, using Student's t-test. ns = not significant at
1115 $p > 0.05$. *StEIF3e* was used as a reference gene. Detection (E) and relative fold change
1116 (F) of mature miR166 from leaves and stolon tissues of SD grown (7 days post
1117 induction, 7 dpi) *Solanum tuberosum* ssp. *andigena* by stem-loop RT-PCR. (G)
1118 Relative abundance of *miR166* in stolon-to-tuber transition stages. StU6 was used for
1119 normalization. Error bars indicate (±) SEM of three biological replicates, each with
1120 three technical replicates. Asterisks (one, two, three, and four) indicate significant
1121 differences at $p < 0.05$, $p < 0.01$, $p < 0.001$, and $p < 0.0001$, respectively, using
1122 Student's t-test. ns = not significant at $p > 0.05$. (H) Confirmation of HD-ZIP III
1123 targets of miR166. Partial mRNA sequence of *ICU1*, *ICU2*, *REV*, *PHB*, *PHV*, and
1124 *HB8* aligned with *miR166*, numbers denote the fraction of cloned cleavage products
1125 that terminate at different positions (arrows).

1126

1127 **Figure 2. Knockdown of microRNA166 causes pleiotropic phenotypic changes** (A)
1128 Expression levels of *miR166* in mimicry lines (KD #2, KD #3) compared to WT. *StU6*
1129 was used as a reference gene. Error bars indicate standard error of means (SEM) from
1130 three biological replicates (n=3). Asterisks (one, two, three, and four) indicate
1131 significant differences at $p < 0.05$, $p < 0.01$, $p < 0.001$, and $p < 0.0001$, respectively,
1132 using Student's t-test. ns = not significant at $p > 0.05$. (B) Plant architecture of
1133 miR166 KD lines along with WT. Scale bar= 5 cm. Plant height (C), number of nodes
1134 (D) and internodal distance (E) of miR166 KD lines in comparison with WT (n=10).
1135 (F) Photographs of 8-week old LD grown plants, showing reduced leaf curvature in
1136 KD plants (arrows). Scale bar= 2 cm. (G) The longitudinal and transverse curvature
1137 indices of leaves emerging from the 5th-node of 8-week old plants (n=10). Asterisks
1138 (one, two, three and four) indicate significant differences at $p < 0.05$, $p<0.01$, $p<0.001$
1139 and $p<0.0001$, respectively, using one-way ANOVA. ns= not significant at <0.05. (H)

1140 Transverse sections of stem from miR166 KD and WT LD grown plants. Scale bar=
1141 50 microns.
1142
1143 **Figure 3. miR166 knockdown lines have reduced tuber productivity** (A)
1144 Representative tuber images from miR166 KD lines compared to WT, each image
1145 contains tubers from 6 plants per line. Scale bar= 2 cm. Tuber weight per plant (B)
1146 and average tuber number (C) of miR166 KD lines compared to WT. Data was taken
1147 from soil grown plants after two months of SD induction, and plotted from 14
1148 individual plants per line. The sphericity index (D) and average tuber volume (E) of
1149 miR166 KD tubers in comparison to WT. The data is plotted for 30 tubers from each
1150 line. Asterisks (one, two, three and four) indicate significant differences at $p < 0.05$,
1151 $p<0.01$, $p<0.001$ and $p<0.0001$, respectively, using one-way ANOVA. ns= not
1152 significant at <0.05. (F) Starch content (mg/gFW) of miR166 KD tubers, relative to
1153 WT tubers. (G) Relative fold change of key tuber marker genes in the stolons (7 days
1154 SD) of miR166 KD, compared to the WT. Error bars indicate standard error of means
1155 (SEM) from three biological replicates (n=3). Asterisks (one, two, three, and four)
1156 indicate significant differences at $p < 0.05$, $p < 0.01$, $p < 0.001$, and $p < 0.0001$,
1157 respectively, using Student's t-test. ns = not significant at $p > 0.05$. (H) *In vitro* tuber
1158 induction assay for miR166 KD lines along with WT.
1159
1160 **Figure 4. RNA-Seq analysis reveals differentially expressed genes in swollen and**
1161 **sub-swollen part of tuberizing stolons** (A) Stolon-to-tuber transition stages as seen
1162 in the WT and miR166 KD #3. (B) A schematic illustration to depict the tissue
1163 collection carried out for RNA-sequencing analysis. The Head and sub-swelling (SSR)
1164 region were collected individually from WT and KD #3 stolons from plants grown
1165 under SD photoperiod for 12 days. (C) Venn diagram shows the summary of unique
1166 and shared genes expressed in KD #3 and WT tissues (Head vs. SSR). Heat map was
1167 plotted for key tuberization pathway genes (D), selective genes from QTLs (E), and
1168 16 genes belonging to the *Ro* locus (F) from WT and KD #3. Numbers inside the box
1169 represent variance-stabilized transformed (VST) values.
1170
1171 **Figure 5. Tuberizing stolons exhibit differential expression of phytohormone-**
1172 **associated genes and differential accumulation of auxin and GA** (A-B) The heat
1173 map represents differential expression of genes involved in Auxin, GA and CK

1174 metabolism and transport. Numbers inside the box represent variance stabilized
1175 transformed (VST) values. (C) Validation of selective auxin biosynthesis genes from
1176 the Head vs. SSR regions. *StEIF3e* was used as reference gene. Error bars indicate
1177 standard error of means (SEM) from three biological replicates (n=3). Asterisks (one,
1178 two, three, and four) indicate significant differences at $p < 0.05$, $p < 0.01$, $p < 0.001$,
1179 and $p < 0.0001$, respectively, using Student's t-test. ns = not significant at $p > 0.05$.
1180 Relative quantification of IAA- 3 (D) and $GA_3$ (E) from the Stolon, Head and SSR
1181 tissues from WT and miR166 KD #3.
1182
1183 **Figure 6. Anthocyanin pathway genes are upregulated in miR166 KD** (A) Tubers
1184 accumulate anthocyanin pigments in their peels. (B) Quantification of Cyanidin 3-
1185 glucoside, pelargonidin 3-glucoside and delphinidin 3-glucoside from the tuber peels
1186 of WT and miR166 KD. The mean value (n = 4) ± SEM is presented. Asterisks (one,
1187 two, three, and four) indicate significant differences at $p < 0.05$, $p < 0.01$, $p < 0.001$,
1188 and $p < 0.0001$, respectively, using one-way ANOVA. ns = not significant at $p > 0.05$.
1189 The RNA-seq analysis showed up regulation of several genes encoding enzymes in
1190 the anthocyanin pathway (C) and some of the TF families having the strong
1191 correlation with these anthocyanin pathway genes (D) (based on Zhang *et al*., 2024)
1192 from the tuberizing stolons of miR166 KD, compared to the WT. Numbers inside the
1193 box represent variance stabilized transformed (VST) values.
1194
1195 **Figure 7. REVOLUTA affects tuberization** (A) Primary PCR product from
1196 modified 5′ RLM-RACE, to confirm *REV* as a target of *miR166* in potato. (B)
1197 Relative fold change of *REV* in differentiating stolons from WT plants. (C) Relative
1198 fold change of *REV* in stolons from miR166 KD and OE lines. *StEIF3e* was used as
1199 reference gene. Error bars indicate standard error of means (SEM) from three
1200 biological replicates (n=3). Asterisks (one, two, three, and four) indicate significant
1201 differences at $p < 0.05$, $p < 0.01$, $p < 0.001$, and $p < 0.0001$, respectively, using
1202 Student's t-test. ns = not significant at $p > 0.05$. (D) Promoter expression of *StREV* in
1203 *promStREV:uidA* transgenic lines. (i) *in vitro* plant, (ii) axillary node, (iii) shoot-
1204 forming stolon, (iv) swollen stolon, (v) T.S. of swollen stolon, and (vi) mini-tuber.
1205 Scale bar= 1000 um for (i) and (vi); Scale bar= 500um for (ii)- (v). Tuber productivity
1206 and tuber numbers (E-G) from REV AS lines, relative to the WT. Scale bar= 2 cm.
1207 Asterisks (one, two, three and four) indicate significant differences at $p < 0.05$, $p<0.01$,

1208 p<0.001 and p<0.0001, respectively, using one-way ANOVA. ns= not significant at
1209 <0.05. (H) Promoters of auxin biosynthesis genes harbor the AT(C/G)AT sequence, a
1210 core motif of HD-ZIP III binding site. (I) Transient infiltration of *REV* in *S.*
1211 *tuberosum* cv. *Désirée* led to reduced expression of *StYUC-4/-7* and *-8*, relative to the
1212 control.
1213
1214 **Figure 8.** A proposed model for the role(s) of miR166-HD-ZIP III module in stolon-
1215 to-tuber transition in potato. miR166 in potato targets the HD-ZIP III transcripts.
1216 REVOLUTA could suppress the expression of auxin biosynthesis genes, and
1217 PHABOLUSA might regulate GA levels, similar to that in soybean (Zhao *et al*.,
1218 2022). Phytohormone dynamics in a developing stolon could regulate the tuber shape
1219 in potato. Auxin-ARF5-HB8 and miR166-HB8/ICU1/2 could influence vascular
1220 differentiation in a tuberizing stolon.

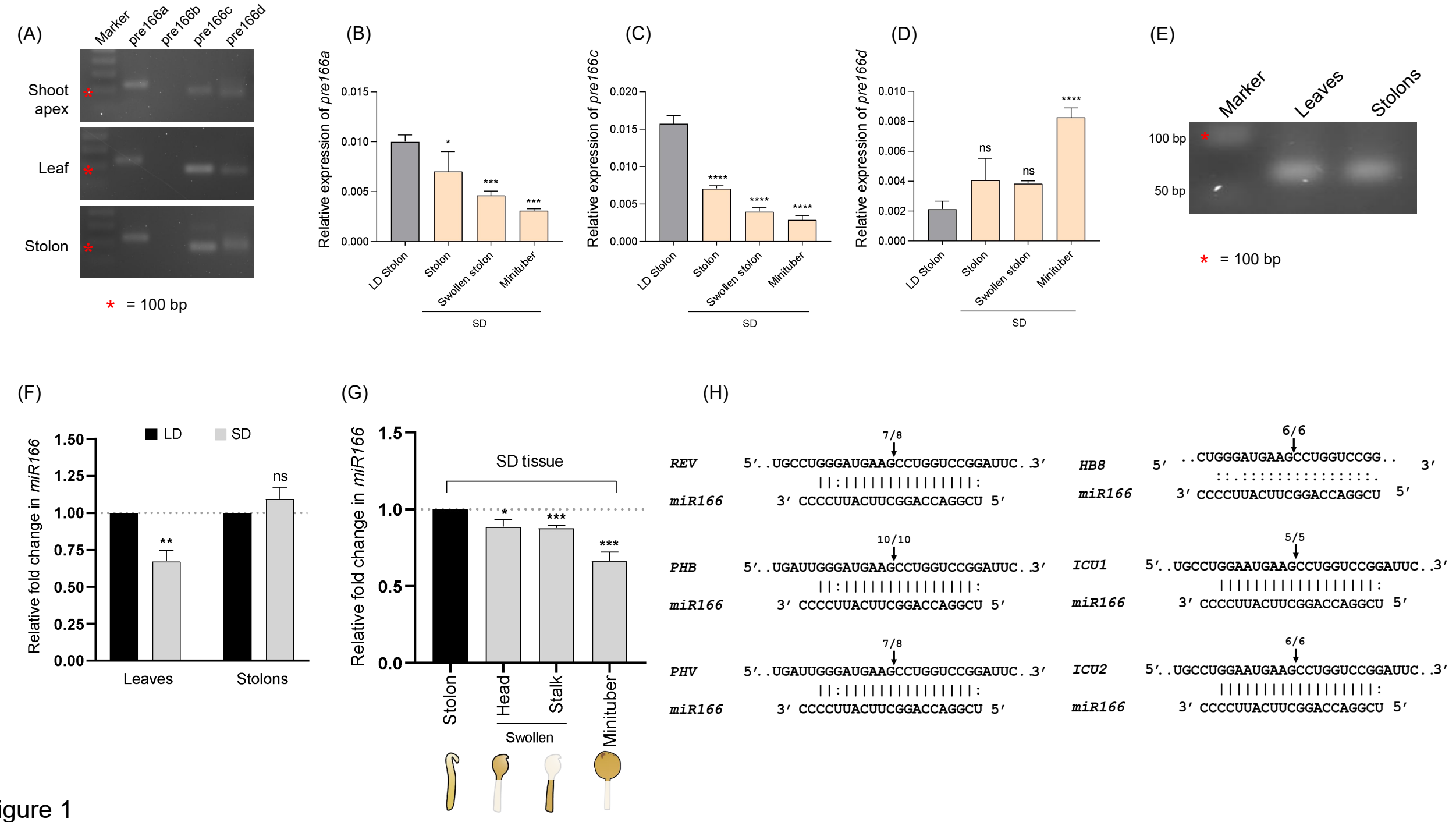
(A)
Marker
pre166a
pre166b
pre166c
pre166d
Shoot apex
Leaf
Stolon
* = 100 bp
(B)
Relative expression of pre166a
0.015
0.010
0.005
0.000
*
***
***
LD Stolon
Stolon
Swollen stolon
Minituber
SD
(C)
Relative expression of pre166c
0.020
0.015
0.010
0.005
0.000
****
****
****
LD Stolon
Stolon
Swollen stolon
Minituber
SD
(D)
Relative expression of pre166d
0.010
0.008
0.006
0.004
0.002
0.000
ns
ns
****
LD Stolon
Stolon
Swollen stolon
Minituber
SD
(E)
Marker
Leaves
Stolons
100 bp
50 bp
* = 100 bp
(F)
LD
SD
Relative fold change in miR166
1.50
1.25
1.00
0.75
0.50
0.25
0.00
**
ns
Leaves
Stolons
(G)
Relative fold change in miR166
1.5
1.0
0.5
0.0
SD tissue
*
***
***
Stolon
Head
Stalk
Minituber
Swollen
(H)
REV 5′..UGCCUGGGAUGAAGCCUGGUCCGGAUUC..3′
7/8
miR166 3′ CCCCUUACUUCGGACCAGGCU 5′
PHB 5′..UGAUUGGGAUGAAGCCUGGUCCGGAUUC..3′
10/10
miR166 3′ CCCCUUACUUCGGACCAGGCU 5′
PHV 5′..UGAUUGGGAUGAAGCCUGGUCCGGAUUC..3′
7/8
miR166 3′ CCCCUUACUUCGGACCAGGCU 5′
HB8 5′ ..CUGGGAUGAAGCCUGGUCCGG.. 3′
6/6
miR166 3′ CCCCUUACUUCGGACCAGGCU 5′
ICU1 5′..UGCCUGGAAUGAAGCCUGGUCCGGAUUC..3′
5/5
miR166 3′ CCCCUUACUUCGGACCAGGCU 5′
ICU2 5′..UGCCUGGAAUGAAGCCUGGUCCGGAUUC..3′
6/6
miR166 3′ CCCCUUACUUCGGACCAGGCU 5′

Figure 1

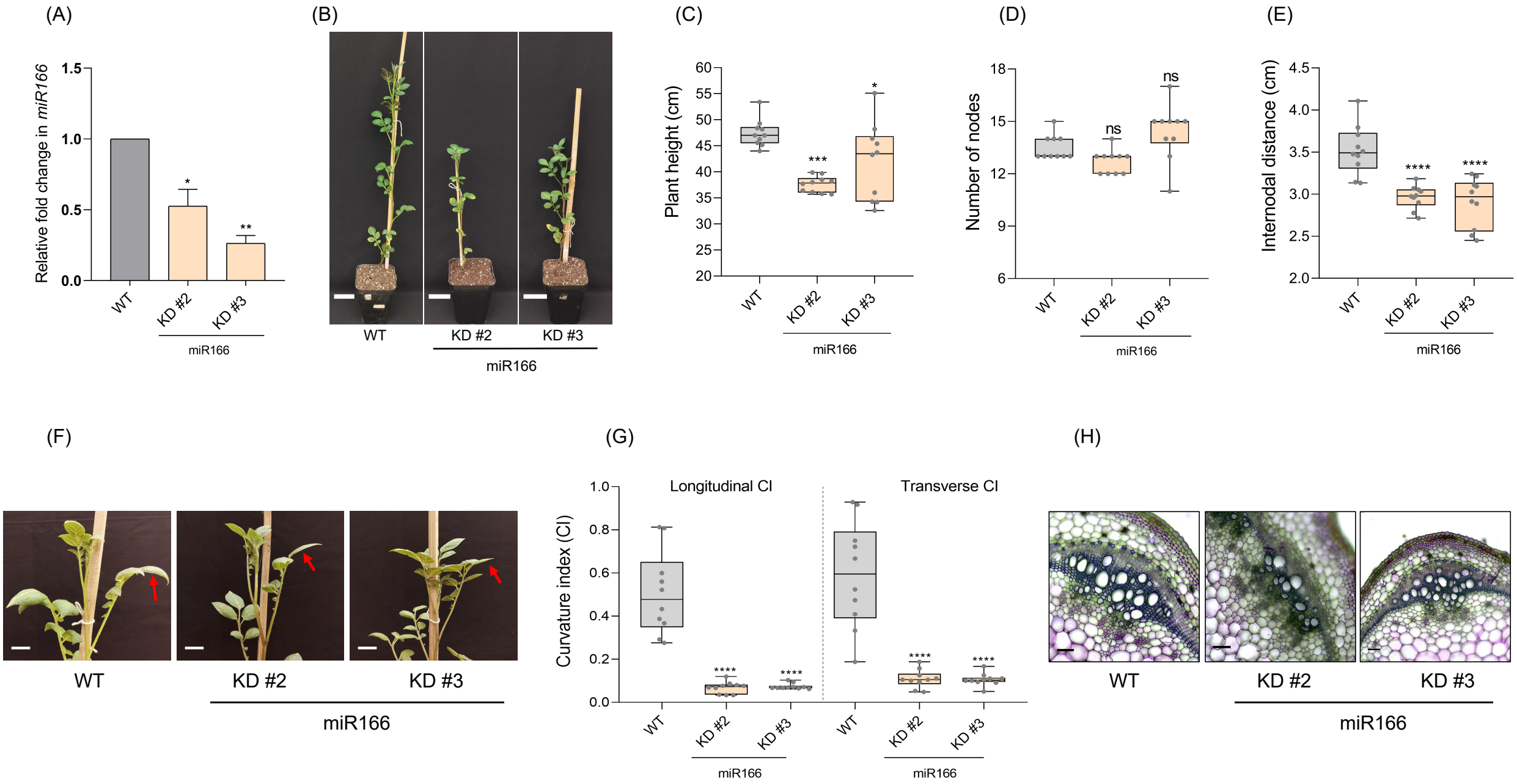
(A)
Relative fold change in miR166
1.5
1.0
0.5
0.0
*
**
WT
KD #2
KD #3
miR166
(B)
WT
KD #2
KD #3
miR166
(C)
Plant height (cm)
60
55
50
45
40
35
30
25
20
***
*
WT
KD #2
KD #3
miR166
(D)
Number of nodes
18
15
12
9
6
ns
ns
WT
KD #2
KD #3
miR166
(E)
Internodal distance (cm)
4.5
4.0
3.5
3.0
2.5
2.0
****
****
WT
KD #2
KD #3
miR166
(F)
WT
KD #2
KD #3
miR166
(G)
Curvature index (CI)
1.0
0.8
0.6
0.4
0.2
0.0
Longitudinal CI
Transverse CI
****
****
****
****
WT
KD #2
KD #3
WT
KD #2
KD #3
miR166
miR166
(H)
WT
KD #2
KD #3
miR166

Figure 2

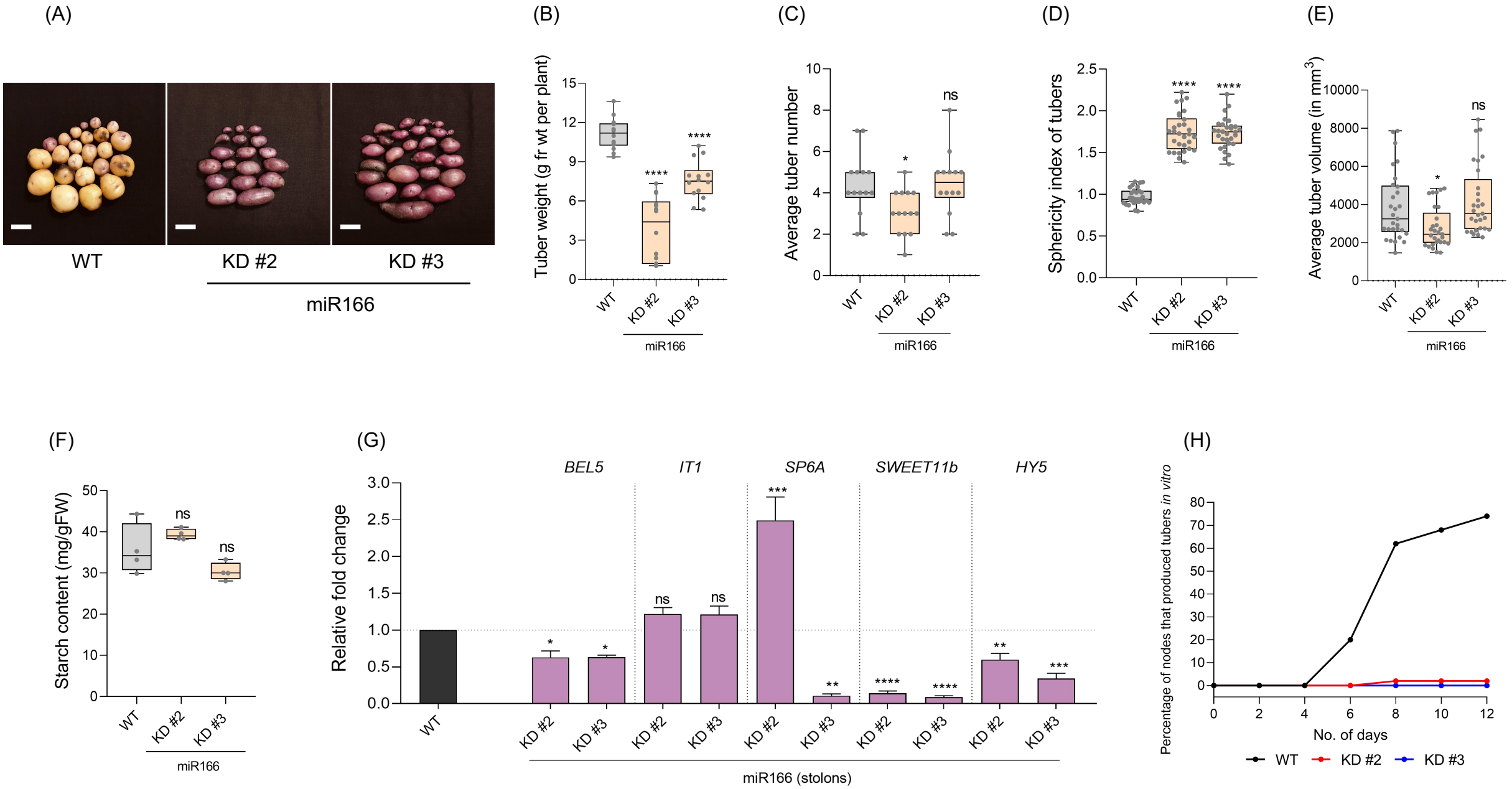
(A)
WT
KD #2
KD #3
miR166
(B)
Tuber weight (g fr wt per plant)
****
****
WT
KD #2
KD #3
miR166
(C)
Average tuber number
ns
*
WT
KD #2
KD #3
miR166
(D)
Sphericity index of tubers
****
****
WT
KD #2
KD #3
miR166
(E)
Average tuber volume (in mm3)
ns
*
WT
KD #2
KD #3
miR166
(F)
Starch content (mg/gFW)
ns
ns
WT
KD #2
KD #3
miR166
(G)
BEL5
IT1
SP6A
SWEET11b
HY5
Relative fold change
WT
KD #2
KD #3
miR166 (stolons)
(H)
Percentage of nodes that produced tubers in vitro
No. of days
WT
KD #2
KD #3

Figure 3

(A)

(B)

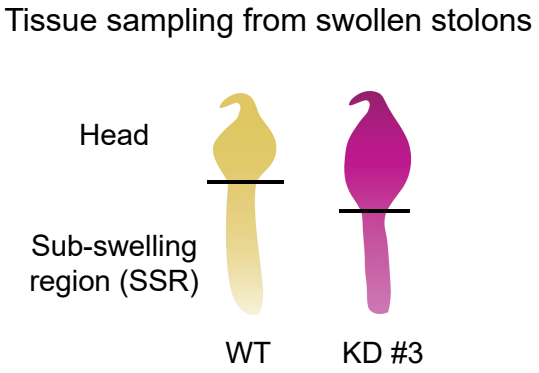


(C)

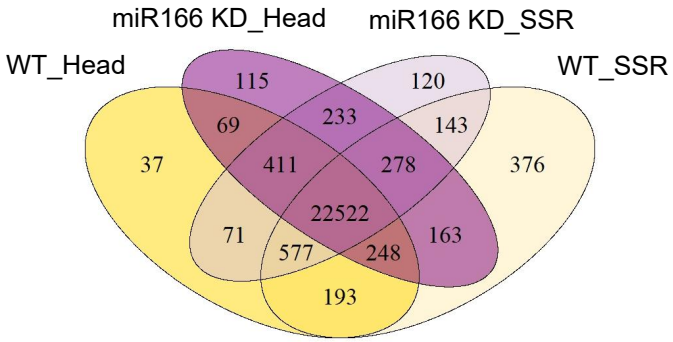


(D)

| | WT_Head | WT_SSR | KD_Head | KD_SSR |
|---|---|---|---|---|
| (BEL5) Soltu.DM.06G029500 | 12.00 | 12.25 | 10.39 | 12.17 |
| (PTB1) Soltu.DM.12G015690 | 11.12 | 10.89 | 10.60 | 10.93 |
| (PTB6) Soltu.DM.10G026670 | 9.40 | 9.29 | 9.35 | 9.17 |
| (CDF1) Soltu.DM.05G005140 | 8.20 | 9.08 | 7.14 | 6.98 |
| (POTH1) Soltu.DM.05G009240 | 7.32 | 8.30 | 7.76 | 7.33 |
| (POTH15) Soltu.DM.02G020620 | 8.68 | 9.62 | 8.44 | 8.47 |
| (SP6A) Soltu.DM.05G026370 | 7.01 | 9.55 | 7.15 | 7.05 |
| (SWEET11b) Soltu.DM.03G019570 | 5.48 | 7.48 | 4.07 | 3.06 |
| (14-3-3) Soltu.DM.12G006890 | 12.17 | 11.24 | 12.64 | 11.99 |
| (BRC1a) Soltu.DM.03G034300 | 8.57 | 10.24 | 7.80 | 7.11 |
| (BRC1b) Soltu.DM.06G025210 | 9.12 | 9.57 | 9.65 | 8.18 |
| (CDPK1) Soltu.DM.12G021650 | 10.53 | 10.83 | 9.91 | 10.59 |
| (PATATIN) Soltu.DM.08G001640 | 15.10 | 14.75 | 16.75 | 18.15 |
| (SP3D) Soltu.DM.03G011110 | 4.21 | 6.43 | 3.96 | 3.26 |
| (SP5G) Soltu.DM.11G004030 | 10.46 | 9.65 | 9.63 | 9.96 |
| (BEL11) Soltu.DM.11G022320 | 12.33 | 13.86 | 11.58 | 12.09 |
| (BEL29) Soltu.DM.01G002850 | 11.67 | 12.59 | 11.13 | 11.63 |
| (CO2) Soltu.DM.02G030260 | 7.61 | 7.77 | 6.05 | 6.38 |
| (BMI1-1) Soltu.DM.09G020810 | 8.07 | 7.63 | 7.43 | 8.18 |
| (E(z)2) Soltu.DM.03G005850 | 10.70 | 10.01 | 9.29 | 9.98 |
| (MSI1) Soltu.DM.01G043650 | 10.56 | 9.54 | 11.12 | 10.79 |

(E)

| QTL genes | WT_Head | KD_Head |
|---|---|---|
| Soltu.DM.05G010370 | 8.04 | 8.29 |
| Soltu.DM.05G010360 | 13.40 | 13.47 |
| Soltu.DM.05G022310 | 4.84 | 4.05 |
| Soltu.DM.10G019120 | 5.68 | 3.21 |
| Soltu.DM.05G009240 | 7.32 | 7.76 |
| Soltu.DM.10G018120 | 10.72 | 9.77 |
| Soltu.DM.10G018140 | 10.69 | 10.23 |
| Soltu.DM.10G018230 | 6.60 | 5.79 |
| Soltu.DM.10G019700 | 7.97 | 9.07 |
| Soltu.DM.10G020110 | 10.43 | 10.47 |
| Soltu.DM.10G020500 | 5.80 | 6.40 |
| Soltu.DM.10G020490 | 7.47 | 6.32 |
| Soltu.DM.10G016590 | 6.89 | 4.48 |
| Soltu.DM.05G023310 | 5.33 | 5.60 |
| Soltu.DM.05G023080 | 8.26 | 7.75 |
| Soltu.DM.12G011130 | 6.21 | 4.52 |
| Soltu.DM.12G011100 | 5.02 | 5.48 |

(F)

| Ro locus | WT_Head | KD_Head |
|---|---|---|
| Soltu.DM.10G018490 | 9.22 | 7.54 |
| Soltu.DM.10G018500 | 6.91 | 5.18 |
| Soltu.DM.10G018510 | 8.77 | 8.67 |
| Soltu.DM.10G018520 | 7.08 | 6.17 |
| Soltu.DM.10G018530 | 10.68 | 10.65 |
| Soltu.DM.10G018550 | 11.43 | 8.18 |
| Soltu.DM.10G018560 | 3.87 | 4.05 |
| Soltu.DM.10G018570 | 9.21 | 10.42 |
| Soltu.DM.10G018580 | 9.82 | 8.95 |
| Soltu.DM.10G018590 | 12.74 | 11.59 |
| Soltu.DM.10G018600 | 9.05 | 8.82 |
| Soltu.DM.10G018610 | 9.76 | 9.48 |
| Soltu.DM.10G018620 | 9.30 | 7.62 |
| Soltu.DM.10G018640 | 8.51 | 7.37 |
| Soltu.DM.10G018650 | 8.49 | 8.09 |
| Soltu.DM.10G018660 | 4.75 | 4.99 |

Figure 4

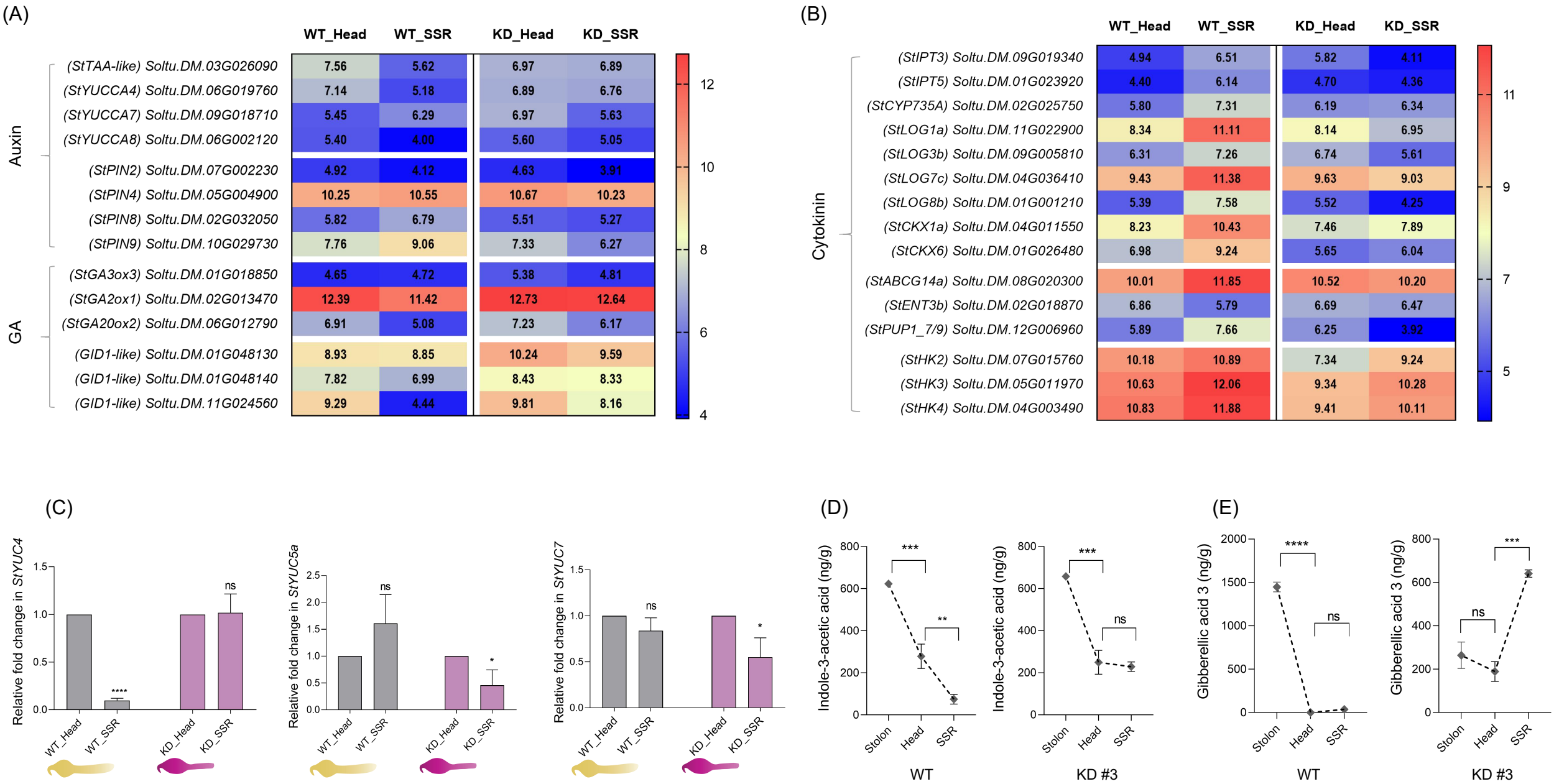
(A)
WT_Head
WT_SSR
KD_Head
KD_SSR
Auxin
(StTAA-like) Soltu.DM.03G026090 7.56 5.62 6.97 6.89
(StYUCCA4) Soltu.DM.06G019760 7.14 5.18 6.89 6.76
(StYUCCA7) Soltu.DM.09G018710 5.45 6.29 6.97 5.63
(StYUCCA8) Soltu.DM.06G002120 5.40 4.00 5.60 5.05
(StPIN2) Soltu.DM.07G002230 4.92 4.12 4.63 3.91
(StPIN4) Soltu.DM.05G004900 10.25 10.55 10.67 10.23
(StPIN8) Soltu.DM.02G032050 5.82 6.79 5.51 5.27
(StPIN9) Soltu.DM.10G029730 7.76 9.06 7.33 6.27
GA
(StGA3ox3) Soltu.DM.01G018850 4.65 4.72 5.38 4.81
(StGA2ox1) Soltu.DM.02G013470 12.39 11.42 12.73 12.64
(StGA20ox2) Soltu.DM.06G012790 6.91 5.08 7.23 6.17
(GID1-like) Soltu.DM.01G048130 8.93 8.85 10.24 9.59
(GID1-like) Soltu.DM.01G048140 7.82 6.99 8.43 8.33
(GID1-like) Soltu.DM.11G024560 9.29 4.44 9.81 8.16
12
10
8
6
4
(B)
WT_Head
WT_SSR
KD_Head
KD_SSR
Cytokinin
(StIPT3) Soltu.DM.09G019340 4.94 6.51 5.82 4.11
(StIPT5) Soltu.DM.01G023920 4.40 6.14 4.70 4.36
(StCYP735A) Soltu.DM.02G025750 5.80 7.31 6.19 6.34
(StLOG1a) Soltu.DM.11G022900 8.34 11.11 8.14 6.95
(StLOG3b) Soltu.DM.09G005810 6.31 7.26 6.74 5.61
(StLOG7c) Soltu.DM.04G036410 9.43 11.38 9.63 9.03
(StLOG8b) Soltu.DM.01G001210 5.39 7.58 5.52 4.25
(StCKX1a) Soltu.DM.04G011550 8.23 10.43 7.46 7.89
(StCKX6) Soltu.DM.01G026480 6.98 9.24 5.65 6.04
(StABCG14a) Soltu.DM.08G020300 10.01 11.85 10.52 10.20
(StENT3b) Soltu.DM.02G018870 6.86 5.79 6.69 6.47
(StPUP1_7/9) Soltu.DM.12G006960 5.89 7.66 6.25 3.92
(StHK2) Soltu.DM.07G015760 10.18 10.89 7.34 9.24
(StHK3) Soltu.DM.05G011970 10.63 12.06 9.34 10.28
(StHK4) Soltu.DM.04G003490 10.83 11.88 9.41 10.11
11
9
7
5
(C)
Relative fold change in StYUC4
Relative fold change in StYUC5a
Relative fold change in StYUC7
ns
****
*
WT_Head
WT_SSR
KD_Head
KD_SSR
(D)
Indole-3-acetic acid (ng/g)
***
**
Stolon
Head
SSR
WT
KD #3
(E)
Gibberellic acid 3 (ng/g)
****
***
ns

Figure 5

(A)

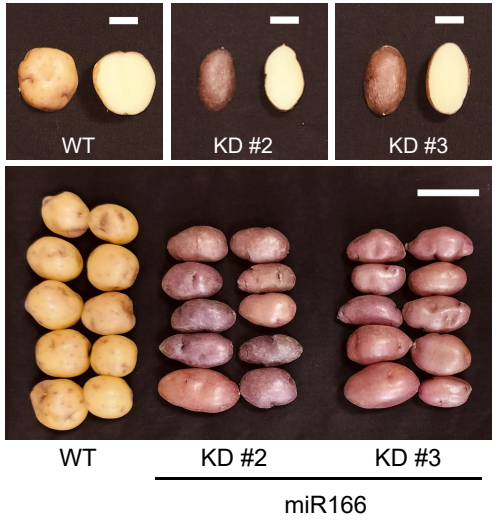


(B)

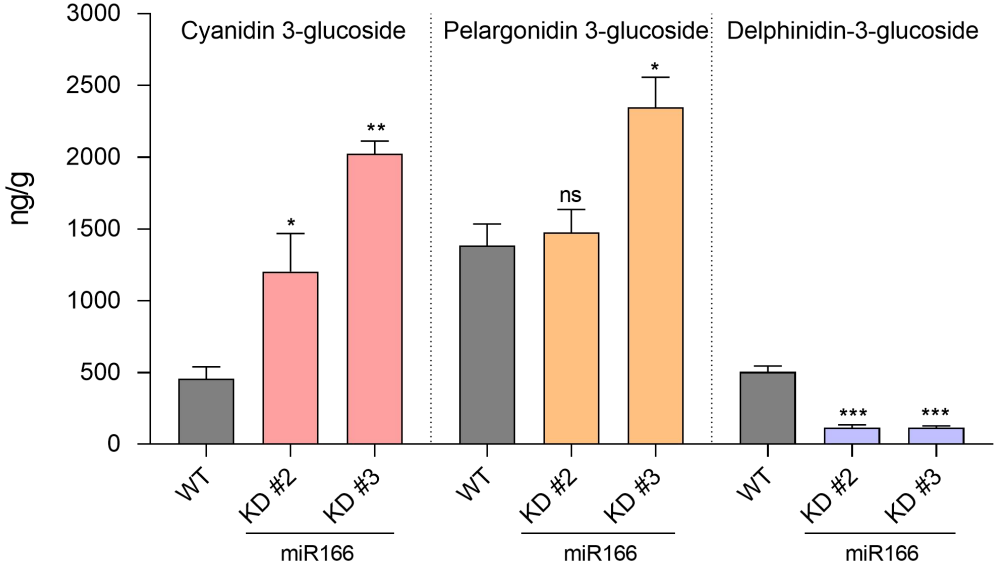


(C)

| | WT_Head | KD_Head |
|---|---|---|
| (GST) Soltu.DM.02G020850 | 11.90 | 13.98 |
| (F3H) Soltu.DM.02G023850 | 10.61 | 11.75 |
| (DFR) Soltu.DM.02G024900 | 12.27 | 12.96 |
| (MATE) Soltu.DM.03G018250 | 11.10 | 12.13 |
| (4CL-2) Soltu.DM.03G020790 | 7.34 | 7.53 |
| (F3'H) Soltu.DM.03G029340 | 7.72 | 8.19 |
| (F3'H-1) Soltu.DM.03G037130 | 8.38 | 9.32 |
| (CHI-1) Soltu.DM.05G001950 | 9.55 | 10.97 |
| (CHI-2) Soltu.DM.05G022280 | 10.72 | 13.03 |
| (CHS-1) Soltu.DM.05G023610 | 9.15 | 12.09 |
| (PAL) Soltu.DM.05G026870 | 9.74 | 11.16 |
| (4CL-1) Soltu.DM.06G024540 | 9.58 | 10.07 |
| (C4H) Soltu.DM.06G032850 | 11.66 | 13.07 |
| (UFGT-1) Soltu.DM.07G014160 | 12.61 | 12.42 |
| (CHI-3) Soltu.DM.07G023150 | 9.83 | 10.32 |
| (ANS-1) Soltu.DM.08G026700 | 11.68 | 13.49 |
| (UFGT-2) Soltu.DM.09G017160 | 11.43 | 12.88 |
| (MT) Soltu.DM.09G025040 | 13.46 | 14.76 |
| (CHS-2) Soltu.DM.09G028560 | 9.33 | 12.79 |
| (F3'5'H-1) Soltu.DM.09G030920 | 6.47 | 7.06 |
| (F3'5'H-2) Soltu.DM.11G020990 | 10.59 | 11.90 |
| (ANS-2) Soltu.DM.11G025090 | 7.41 | 7.78 |
| (4CL-3) Soltu.DM.12G004930 | 8.35 | 7.73 |

(D)

| | WT_Head | KD_Head |
|---|---|---|
| (RAV) Soltu.DM.03G022370 | 5.11 | 3.93 |
| (WRKY) Soltu.DM.01G030510 | 8.22 | 9.27 |
| (bHLH) Soltu.DM.01G035540 | 9.95 | 10.09 |
| (bZIP) Soltu.DM.01G049720 | 11.81 | 13.04 |
| (Dof) Soltu.DM.02G016040 | 7.12 | 8.07 |
| (WRKY) Soltu.DM.03G013350 | 6.16 | 6.93 |
| (bZIP) Soltu.DM.04G026750 | 8.57 | 8.40 |
| (WRKY) Soltu.DM.07G017160 | 8.34 | 7.91 |
| (GRAS) Soltu.DM.07G018410 | 10.10 | 10.60 |
| (E2F/DP) Soltu.DM.09G002290 | 7.17 | 7.58 |
| (bHLH) Soltu.DM.09G019660 | 7.51 | 8.30 |
| (WRKY) Soltu.DM.10G021890 | 5.12 | 6.62 |
| (bZIP) Soltu.DM.10G030340 | 7.11 | 6.79 |
| (Trihelix) Soltu.DM.11G000160 | 7.76 | 7.93 |
| (LBD) Soltu.DM.11G025680 | 7.76 | 7.26 |
| (ARF) Soltu.DM.05G026740 | 9.05 | 8.24 |
| (ARF) Soltu.DM.06G030530 | 8.17 | 7.35 |
| (B3) Soltu.DM.02G008680 | 8.10 | 7.43 |
| (B3) Soltu.DM.06G002620 | 8.26 | 8.73 |
| (AP2) Soltu.DM.08G028420 | 5.81 | 4.94 |
| (ERF) Soltu.DM.03G005790 | 8.98 | 10.93 |
| (G2-like) Soltu.DM.06G019150 | 9.42 | 9.83 |
| (HB-other) Soltu.DM.12G027800 | 8.50 | 9.55 |
| (HD-ZIP) Soltu.DM.03G027170 | 11.32 | 11.83 |
| (HD-ZIP) Soltu.DM.04G030250 | 9.91 | 11.17 |
| (MYB) Soltu.DM.03G014050 | 6.59 | 7.83 |
| (MYB) Soltu.DM.05G004700 | 6.89 | 9.59 |
| (MYB) Soltu.DM.10G020850 | 10.75 | 12.31 |
| (MYB_related) Soltu.DM.01G035880 | 12.01 | 11.56 |

Figure 6

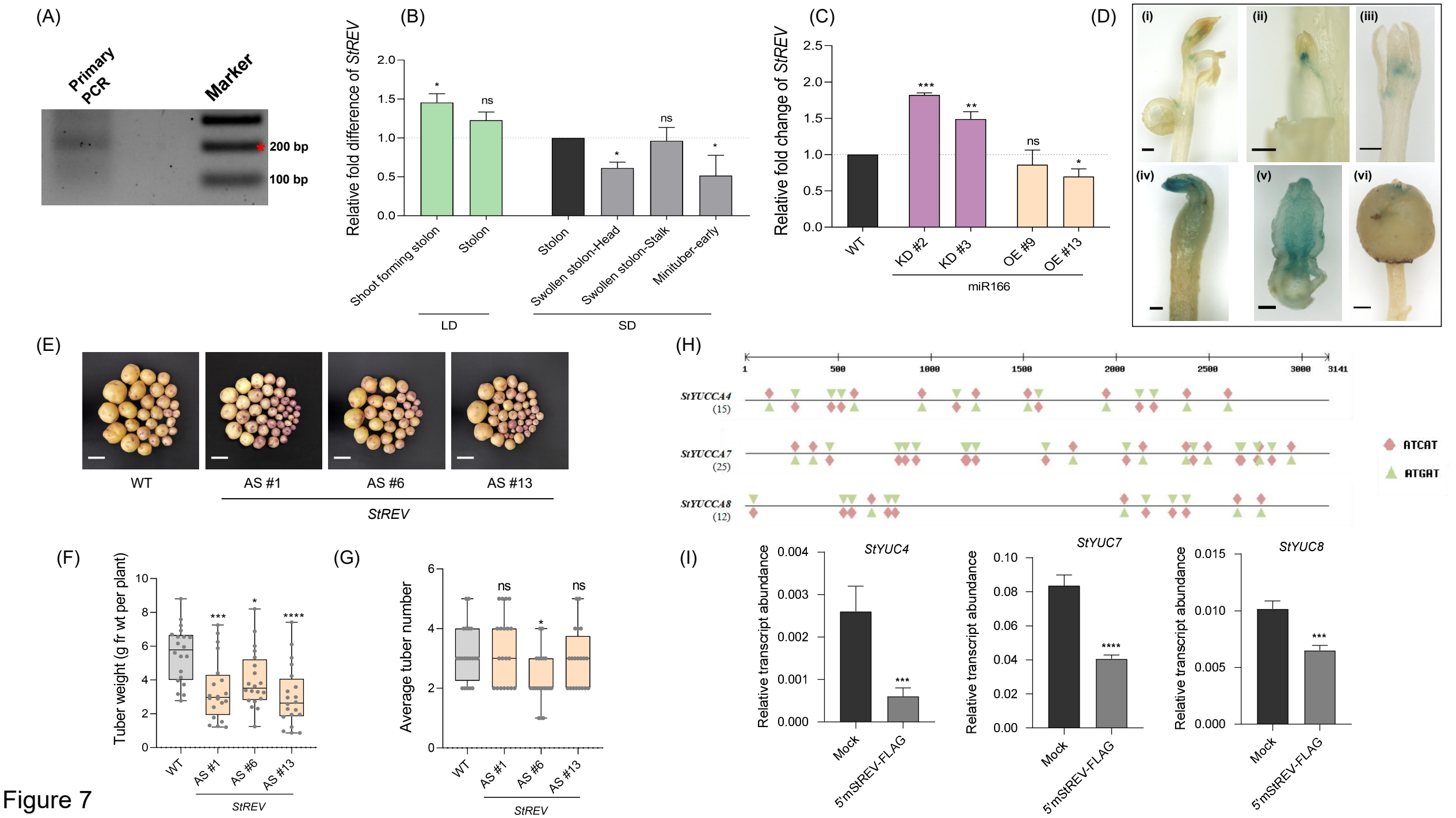
(A)
Primary PCR
Marker
200 bp
100 bp
(B)
Relative fold difference of StREV
Shoot forming stolon
Stolon
Stolon
Swollen stolon-Head
Swollen stolon-Stalk
Minituber-early
LD
SD
(C)
Relative fold change of StREV
WT
KD #2
KD #3
OE #9
OE #13
miR166
(D)
(i)
(ii)
(iii)
(iv)
(v)
(vi)
(E)
WT
AS #1
AS #6
AS #13
StREV
(H)
StYUCCA4
StYUCCA7
StYUCCA8
ATCAT
ATGAT
(F)
Tuber weight (g fr wt per plant)
(G)
Average tuber number
(I)
StYUC4
StYUC7
StYUC8
Relative transcript abundance
Mock
5'mStREV-FLAG

Figure 7

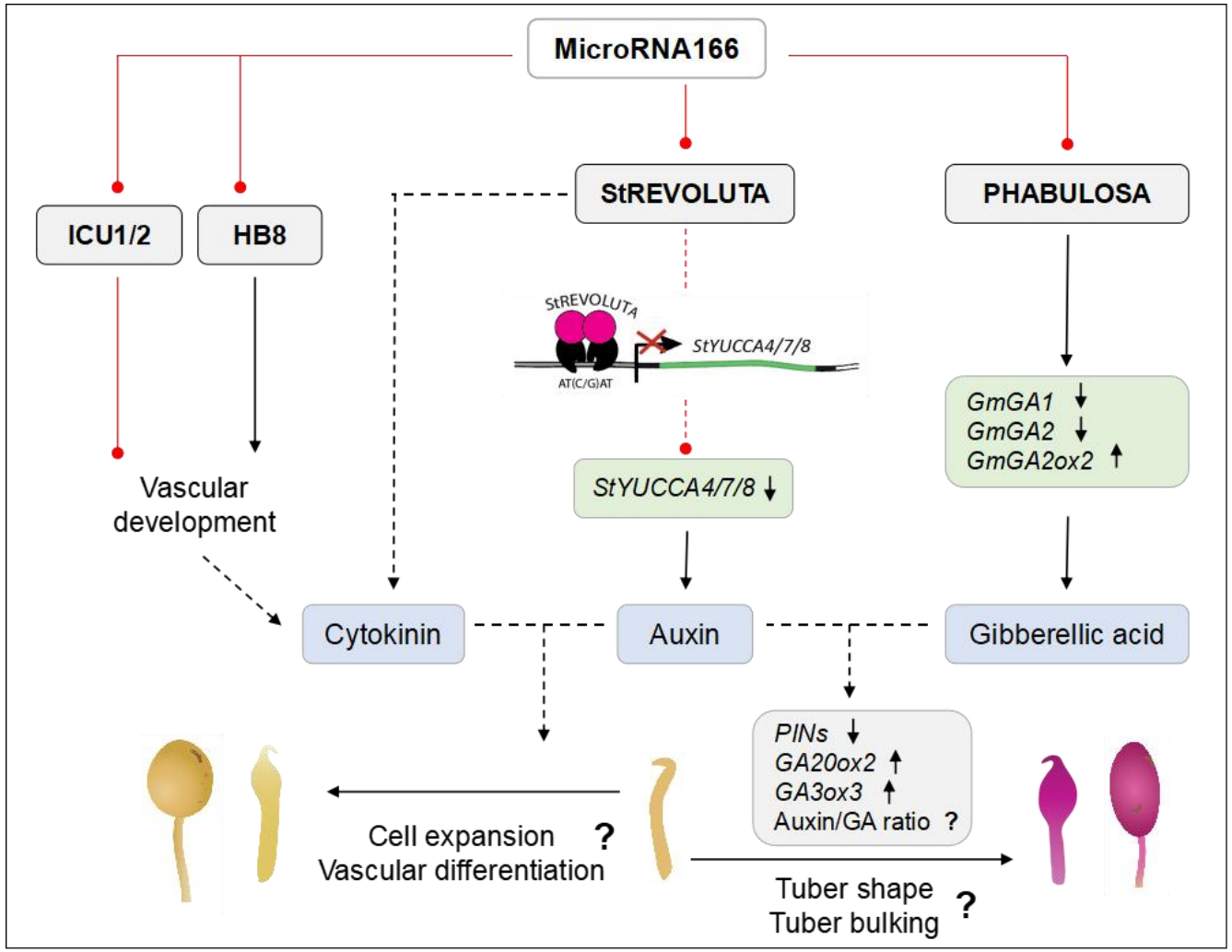


Proposed model for the role(s) of miR166-HD-ZIP III module in potato tuber development

Figure 8